Available online at www.sciencedirect.com
SCIENCE DIRECT
Journal of Sound and Vibration 295 (2006) 659–684
JOURNAL OF SOUND AND VIBRATION
www.elsevier.com/locate/jsvi

Experimental and theoretical study of gust response for a wing–store model with freeplay

Deman Tang, Earl H. Dowell*

Department of Mechanical Engineering and Materials Science, Duke University, Durham, North Carolina 27708-0300, USA

Received 7 September 2004; received in revised form 19 December 2005; accepted 14 January 2006
Available online 29 March 2006

Abstract

An experimental delta wing/store model with freeplay in a periodic gust field has been designed and tested in the Duke wind tunnel. The wing structure is modeled theoretically using von Karman plate theory that accounts for geometric strain–displacement nonlinearities in the plate wing structure. A component modal analysis is used to derive the full structural equations of motion for the wing/store system. A 3-D time domain vortex lattice aerodynamic model including a reduced order model aerodynamic technique and a slender body aerodynamic theory for the store are also used to investigate the nonlinear aeroelastic system. The effects of the freeplay gap, the gust angle of attack and the initial conditions on the gust response are discussed. The quantitative correlations between the theory and experiment are reasonably good, but in the range of the dominant resonant frequency of this nonlinear system, i.e. at larger response amplitudes, the correlations are not good. The theoretical structural model needs to be improved to determine larger amplitude motions near the resonant frequency.

1. Introduction

The emphasis in the field of aeroelasticity is on the interaction among aerodynamic, structural elastic and inertia forces. Limit cycle oscillations (LCO), or nonlinear aeroelastic responses, have received particular attention in recent years. For a more in-depth discussion of these issues, see a recent review paper [1]. Much of the literature is concerned with self-excited oscillations, i.e. flutter and the associated LCO. However, nonlinear aeroelastic response of an aircraft operating in a gust field is also of interest. The gust source is atmospheric turbulence usually modeled as a random gust or a periodic gust. In the late 1980s, the Federal Aviation Administration requested assistance from NASA for initial evaluation of a candidate method for analysis of gust loads on aircraft with nonlinearities. The statistical discrete gust (SDG) method [2] has been proposed to permit analysis of nonlinear aircraft models for gust loads. As a time-domain method, it also permits the computation of time-correlated gust loads. NASA conducted an evaluation of the SDG method, focusing on its relationship to existing linear methods [3]. Optimization of a wing structure for gust response [4] using the computer code ASTROS [5] and a study of gust alleviation using state-space aeroelastic modeling

*Corresponding author. Tel.: +1 919 660 5302; fax: +1 919 660 0089.
E-mail address: dowell@ee.duke.edu (E.H. Dowell).

0022-460X/$ - see front matter © 2006 Elsevier Ltd. All rights reserved.
doi:10.1016/j.jsv.2006.01.024

Nomenclature

a_i, b_j	generalized coordinates in x- and y-directions, respectively
c	delta wing root chord
D	delta wing plate bending stiffness
d	nondimensional freeplay gap of the store, δ/h
E	Young's modulus
h	delta wing plate thickness
km, kn	numbers of vortex elements on delta wing in x- and y-directions, respectively
kmm	total number of vortices on both the delta wing and wake in the x-direction
L	delta wing span
m	delta wing panel mass/area, $m = h\rho_m$
mxy	number of delta wing modal functions in the x- and y-plane defining u, v
nxy	number of delta wing modal functions in the z-direction defining w
$q, \dot{q}$	state-space vector
q_n	generalized coordinate in the z-direction
Q^{ij}	generalized aerodynamic force
R_a	size of reduced order aerodynamic model
t	time
U	airspeed
u, v	in-plane displacements
U_i, V_j	modal functions in x- and y-directions
w	plate transverse deflection
w_g, w_{g0}	nondimensional lateral gust velocity and amplitude
W_k	transverse modal function in z-direction
x, y	streamwise and spanwise coordinates
X, Y	right and left eigenvector matrices of vortex lattice eigenvalue model
z	normal coordinate
α_g	gust angle of attack
α_{g0}	gust angle amplitude for a sinusoid gust
α_{g1}, α_{g2}	first and second gust angle amplitudes for a measured gust
β	store pitch angle
δ	freeplay gap of the store
Δp	aerodynamic pressure loading on panel
$\overline{\Delta p}$	nondimensional aerodynamic pressure, $\Delta p/(\rho_\infty U^2)$
Δt	time step, $\Delta x/U$
Δx	plate element length in the streamwise direction
γ	reduced vortex strength
Γ	vortex strength
ν	Poisson's ratio
ω_g	gust frequency
ρ_∞, ρ_m	air and plate densities
θ	state-space vector
τ	time parameter, $\sqrt{mc^4/D}$
$(\dot{})$	$\mathrm{d}()/\mathrm{d}t$

[6] have been proposed. These studies have made significant contributions to gust response methods for treating real aircraft.

In previous work, the present authors and colleagues have used a series of relatively low-cost, simple aeroelastic models of a wing, wing/store and a typical airfoil to study the fundamental mechanisms of nonlinear aeroelastic response to a gust. To create an experimental gust field, a rotating slotted cylinder (RSC) gust generator was designed and installed in the Duke University low-speed wind tunnel based upon a concept developed by W.H. Reed III. Either a sinusoidal gust or a linear frequency sweep gust excitation can be produced. This gust field can also simulate turbulence with a uniform power spectral density over a certain frequency band in the lateral and longitudinal directions [7].

A nonlinear gust response analysis and correlation with wind tunnel tests of a typical airfoil section with control surface freeplay model were made [8]. An electro-magnetic dry friction damper was also designed, manufactured and installed in this airfoil. The nonlinear damper can be used to alleviate the dynamic response to both a periodic and a linear frequency sweep gust excitation, especially for the plunge and pitch response of the three degrees of freedom airfoil model [9,10].

A high-aspect-ratio wing model was also studied with structural equations of motion based on nonlinear beam theory combined with the ONERA aerodynamic stall model. The effects of geometric structural nonlinearity and steady angle of attack on nonlinear gust response of a high-aspect-ratio wing were considered [11,12]. Other related work for the high-aspect-ratio wing model studied the nonlinear response to lateral turbulence in sinusoidal pulsating flow created by the RSC gust generator. This gust field was also used to simulate a rotor blade operating condition [13,14]. Again theory and experiment showed good correlation.

A 3-D low-aspect-ratio wing (delta wing) model was made as well. Structural equations of motion based on a nonlinear plate theory (von Karman plate equations) were combined with a 3-D time domain vortex lattice aerodynamic model (linear model). A reduced order aerodynamic technique was used to investigate the nonlinear aeroelastic response and the effects of steady angle of attack. Results were obtained and correlated from both theoretical and experimental studies [15,16].

Most recently, and following the work of Tang et al. [15], an experimental model with a wing/store model with and without freeplay has been designed [17,18] for the study of flutter and LCO. The wing is modeled as a simple plate of constant thickness. The store is modeled as a slender rigid body that contacts the wing through two support points. The fore support point is articulated to the wing and the aft support point contacts the wing through a spring with a freeplay gap. The store is assumed to have motion relative to the wing in only one degree of freedom (dof), i.e. in pitch. Thus the store itself is a single dof excited by nonlinear forces from the wing through the two support points and the freeplay gap. In the present paper, we develop a mathematical model and computational code in the time domain to calculate the nonlinear gust response of a delta wing/store model with a store pitch freeplay gap at low subsonic flow speeds. Sinusoidal and linear frequency sweep gust loads are considered. A 3-D time domain vortex lattice aerodynamic model combined with a reduced order model aerodynamic technique and a slender body aerodynamic theory for the store are used to investigate the nonlinear aeroelastic system.

In order to validate the theoretically predicted gust response characteristics of the delta wing/store model, an experimental investigation has been carried out in the Duke wind tunnel using a RSC gust generator. The results may be helpful in better understanding physically the nonlinear aeroelastic response of a delta wing/store model with freeplay to gust loads and the capability of von Karman nonlinear plate theory for describing the gust response of this experimental model.

2. State-space equations

A schematic of the delta wing-plate/store geometry is shown in Fig. 1(a) and a photograph of the experimental delta wing-plate/store model and gust generator in the wind tunnel is shown in Fig. 1(b).

The aeroelastic structure/fluid state-space equations are described next.

2.1. Nonlinear structural model

A component modal analysis [19] is used to derive the full structural equations of motion for the wing/store combination system.

The plate wing and store structures can be viewed as separate components that can be analyzed individually and then joined through an appropriate constraint function. The full structural equations of motion can thus be obtained in a very compact form. The kinetic, potential energies and the generalized nonconservative work of the plate wing are based upon the von Karman plate theory as discussed in Ref. [15]

The classical Rayleigh–Ritz approach will be used here. In the Rayleigh–Ritz approach the original displacement variables, u, v, w, which are functions of x, y and t are expanded in a series of the product of time-dependent modal coordinates and space-dependent global functions. We expand the transverse or out-of-plane displacement, w and the in-plane displacements u and v, as follows:

$$u(x,y,t) = \sum_m a_m(t) U_m(x,y), \quad m = 1 \ldots mxy, \tag{1}$$

$$v(x,y,t) = \sum_n b_n(t) V_n(x,y), \quad n = 1 \ldots mxy, \tag{2}$$

$$w(x,y,t) = \sum_k q_k(t) \psi_k(x,y), \quad k = 1 \ldots nxy, \tag{3}$$

where the transverse natural mode function, $\psi_k(x,y)$ is calculated using a 2-D finite-element method for the delta wing plate. The in-plane natural mode functions, $U_i(x,y)$ and $V_j(x,y)$, are calculated by a 3-D finite-element method. All such calculations are done using a standard computational code, ANSYS [20]. These functions satisfy the boundary conditions (partial root clamp) of the cantilevered delta wing.

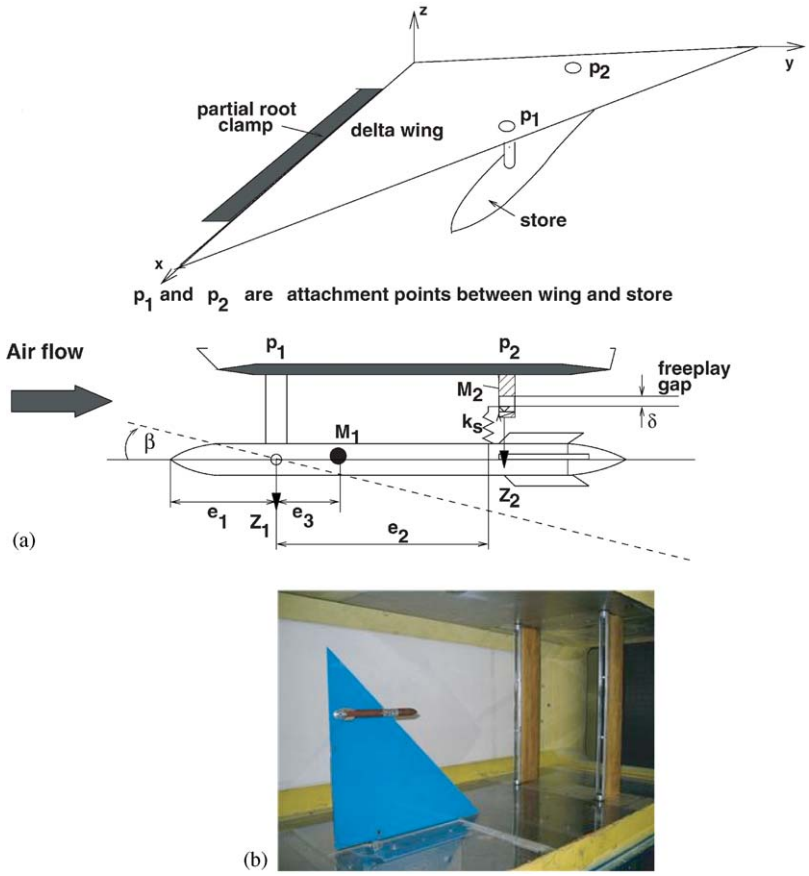

Fig. 1. A delta wing model with an external store in the wind tunnel: (a) schematic diagram of wing/store model, (b) photograph of wing/store model.

The potential energy of the store is expressed as

$$\begin{cases} V^{\beta} = \frac{1}{2}k_s(Z_1 + \beta e_2 - Z_2)^2, \\ k_s = \begin{cases} k_{so} & \text{if } |Z_1 + \beta e_2 - Z_2| \geqslant \delta, \\ 0 & \text{otherwise,} \end{cases} \end{cases} \tag{4}$$

where k_{so}, δ are the attachment stiffness between the wing and store at the aft attached point and the corresponding freeplay gap, respectively.

The kinetic energy of the store is

$$T^{\beta} = \tfrac{1}{2}(M_1\dot{Z}_1^2 + M_2\dot{Z}_2^2 + J_{\beta}\dot{\beta}^2). \tag{5}$$

The generalized nonconservative work for the store can be expressed as

$$\delta W^{\beta} = M^{\beta}\delta\beta. \tag{6}$$

In Eqs. (4)–(6) (p_1) (fore) and (p_2) (aft) are the attachment points between the wing and the store; M_1 is the mass of the store and M_2 is the mass at the aft attachment point, Z_1 and Z_2 are the displacements of the fore and aft attachment points of the store, respectively. e_2 and e_3 are the distances between fore and aft attachment points of the store and between the fore attachment point and the mass center of the store, respectively. M^{β} is a aerodynamic moment loading on the store.

The constraint conditions in the fore and aft attached points between the wing and the store may be expressed as

$$f_1 \equiv \sum_{k=1}^{nxy} q_k \psi_k(p_1) - Z_1 = 0, \tag{7}$$

$$f_2 \equiv \sum_{k=1}^{nxy} q_k \psi_k(p_2) - Z_2 = 0. \tag{8}$$

The Lagrangian is

$$L = T - V + \sum_{i=1}^{2} \lambda_i f_i = T^p + T^\beta - V^p - V^\beta + \lambda_1 f_1 + \lambda_2 f_2,$$

where λ_i are Lagrange multipliers.

Lagrange's equations for this constrained system are derived with respect to $q_k, Z_1, Z_2, \lambda_1, \lambda_2$ and β to obtain the following six sets of equations:

$$m_k[\ddot{q}_k + (\omega_k)^2 q_k] - Q^k - F^\beta + F_N^k = \lambda_1 \psi_k(p_1) + \lambda_2 \psi_k(p_2), \tag{9}$$

$$M_1 \ddot{Z}_1 + k_s(Z_1 - Z_2 + e_2\beta) = -\lambda_1, \tag{10}$$

$$M_2 \ddot{Z}_2 + k_s(Z_2 - Z_1 - e_2\beta) = -\lambda_2, \tag{11}$$

$$J_\beta \ddot{\beta} + k_s e_2^2 \beta + k_s(Z_1 - Z_2) - M^\beta = 0, \tag{12}$$

$$\sum_{k=1}^{nxy} q_k \psi_k(p_1) - Z_1 = 0, \tag{13}$$

$$\sum_{k=1}^{nxy} q_k \psi_k(p_2) - Z_2 = 0, \tag{14}$$

where F_N^k is a nonlinear force which depends upon the deflection of wing, i.e.

$$F_N^k = \sum_{m=1}^{mxy} \sum_{l=1}^{nxy} a_m q_l K1_{mlk} + \sum_{n=1}^{mxy} \sum_{l=1}^{nxy} b_n q_l K2_{nlk} + \sum_{r=1}^{nxy} \sum_{s=1}^{nxy} \sum_{t=1}^{nxy} q_r q_s q_t K3_{rstk},$$

Q^k, F^β, M^β are the generalized aerodynamic forces on the wing and on the store.

Eliminating Z_1, Z_2, λ_1 and λ_2, from the above equations, one obtains

$$m_k \ddot{q}_k + M_1 \psi_k(p_1) \sum_{k=1}^{nxy} \ddot{q}_k \psi_k(p_1) + M_2 \psi_k(p_2) \sum_{k=1}^{nxy} \ddot{q}_k \psi_k(p_2) + m_k \omega_k^2 q_k + k_s \Delta\psi_k \left[\sum_{k=1}^{nxy} q_k \Delta\psi_k - e_2\beta \right] = Q^k - F_N^k + F^\beta \psi_k(p_1), \quad k = 1 \ldots nxy, \tag{15}$$

$$J_\beta \ddot{\beta} + k_s e_2^2 \beta - k_s e_2 \sum_{k=1}^{nxy} q_k \Delta\psi_k = M^\beta + M_1 e_3, \tag{16}$$

$$k_s = \begin{cases} k_{so} & \text{if } |\beta e_2 - \sum_{k=1}^{nxy} q_k \Delta\psi_k| \geqslant \delta, \\ 0 & \text{otherwise,} \end{cases} \tag{17}$$

where $\Delta\psi_k \equiv \psi_k(p_2) - \psi_k(p_1)$.

Lagrange's equations for this constrained system are also derived with respect to a_m, b_n to obtain the following two sets of equations:

$$\sum_{i=1}^{mxy} a_i A1_{im} + \sum_{j=1}^{mxy} b_j B1_{jm} = \sum_{l=1}^{nxy}\sum_{o=1}^{nxy} q_l q_k C1_{lkm}, \quad m = 1 \ldots mxy, \tag{18}$$

$$\sum_{i=1}^{mxy} a_i A2_{in} + \sum_{j=1}^{mxy} b_j B2_{jn} = \sum_{l=1}^{nxy}\sum_{o=1}^{nxy} q_l q_k C2_{lkn}, \quad n = 1 \ldots mxy. \tag{19}$$

Note that the store (slender body) drag is neglected in the present analysis.

2.2. Aerodynamic model

2.2.1. Vortex lattice aerodynamic model for the delta wing

A spanwise uniform periodic lateral gust is used, i.e. the gust velocity is only a function of chordwise position and time, $w_g = w_g(x, t)$, and it is normalized by airspeed, U. The gust wavelength is defined as

$$l_g = U/\omega,$$

where ω is the gust excitation frequency, rad/s.

A continuous sinusoidal gust time history at the x_i position on the delta wing can be expressed as

$$w_g(x, t) = w_{g0} \sin(\omega t - \Delta\phi), \tag{20}$$

where a phase difference is defined as $\Delta\phi = x_i/l_g$, or $\Delta\phi = kx_i/C_{SB}$, where C_{SB} is the chord of the store and k is a reduced frequency, $k = \omega C_{SB}/U$.

The flow about the cantilever wing is assumed to be incompressible, inviscid and irrotational. Here, we use an unsteady vortex lattice method to model this flow. The delta wing and wake are divided into a number of elements. In the wake and on the wing all the elements are of equal size, Δx, in the streamwise direction. Point vortices are placed on the plate and in the wake at the quarter chord of the elements. At the three-quarter chord of each plate element a collocation point is placed for the downwash, i.e. we require the velocity induced by the discrete vortices to equal the total downwash arising from the unsteady motion of the delta wing and also the gust. Thus we have the relationship,

$$\mathrm{d}w_i^{t+1} = \left(\frac{\partial w_i}{\partial t}\right)^{t+1} + U\left(\frac{\partial w_i}{\partial x}\right)^{t+1} + w_{g,i}^{t+1}, \quad i = 1, \ldots, km, \tag{21}$$

where $\mathrm{d}w_i^{t+1}$ is the total downwash at the ith collocation point at time step $t+1$. An aerodynamic matrix equation is given by

$$A\Gamma^{t+1} + B\Gamma^{t} = T\,\mathrm{d}w^{t+1}, \tag{22}$$

where A and B are aerodynamic coefficient matrices, see Ref. [21], and $[T]$ is a transfer matrix for determining the relationship between the global vortex lattice mesh and local vortex lattice mesh on the delta wing plate.

From the fundamental aerodynamic theory, we can obtain the pressure distribution on the plate at the jth point in terms of the vortex strengths. The aerodynamic pressure is given by

$$\Delta p_j = \frac{\rho_\infty}{\Delta x}\left[U(\Gamma_j^{t+1} + \Gamma_j^t)/2 + \sum_i^j \Delta x(\Gamma_i^{t+1} - \Gamma_i^t)/\Delta t\right] \tag{23}$$

and the aerodynamic generalized force is calculated from

$$Q^k = \int\int \Delta p \psi_k \,\mathrm{d}x\,\mathrm{d}y = \sum_{j=1}^{NN} \Delta p_j \psi_k(x_j, y_j)\Delta x\,\Delta y. \tag{24}$$

2.2.2. Slender body aerodynamic model for the store

The vertical displacement at any point of the store is

$$Z_a = -Z_1 - \beta[x_\beta - e_1], \tag{25}$$

where e_1 is the distance from leading edge to the elastic axis of the slender body. x_β is the chordwise position of the store. Here Z_1, +up, and β, +nose up and $w_g(x_\beta, t)$ is a gust velocity. Now the downwash or convected vertical velocity is

$$w_a(x_\beta, t) = \frac{\partial Z_a}{\partial t} + U\frac{\partial Z_a}{\partial x_\beta} + w_g(x_\beta, t). \tag{26}$$

We follow Bisplinghoff et al. [22],

$$\frac{\mathrm{d}F^\beta}{\mathrm{d}x_\beta} = -\rho_\infty \frac{DS}{Dt}\left[\frac{\partial Z_a}{\partial t} + U\frac{\partial Z_a}{\partial x_\beta} + w_g(x_\beta, t)\right] - \rho_\infty S\left[\frac{D}{Dt}\left(\frac{\partial Z_a}{\partial t}\right) + U\frac{D}{Dt}\left(\frac{\partial Z_a}{\partial x_\beta}\right) + \frac{Dw_g}{Dt}\right], \tag{27}$$

where $D/Dt \equiv \partial/\partial t + U\,\partial/\partial x_\beta$, $S \equiv$ body cross-sectional area and $S = \pi R^2$, for a circular cross-section of radius, $R(x_\beta)$.

Note that

$$\frac{DS}{Dt} = U\frac{\mathrm{d}S}{\mathrm{d}x_\beta}.$$

Then Eq. (27) becomes

$$\frac{\mathrm{d}F^\beta}{\mathrm{d}x_\beta} = -\rho_\infty U\frac{\mathrm{d}S}{\mathrm{d}x_\beta}\left(\frac{DZ_a}{Dt} + w_g\right) - \left(\rho_\infty S\frac{D^2Z_a}{Dt^2} + \frac{Dw_g}{Dt}\right). \tag{28}$$

Now, $F^\beta \equiv \int_0^{c_{SB}} (\mathrm{d}F^\beta/\mathrm{d}x_\beta)\,\mathrm{d}x_\beta$ and $M^\beta \equiv \int_0^{c_{SB}} \mathrm{d}F^\beta/\mathrm{d}x_\beta[x_\beta - e_1]\,\mathrm{d}x_\beta$, where $c_{SB} \equiv$ chord of slender body.

Finally,

$$F^\beta = \rho_\infty[\ddot{Z}_1 + U\dot{\beta}]\int_0^{c_{SB}} S\,\mathrm{d}x_\beta + \rho_\infty\ddot{\beta}\int_0^{c_{SB}} S[x_\beta - e_1]\,\mathrm{d}x_\beta + F_g^\beta \tag{29}$$

and

$$M^\beta = \rho_\infty U[\dot{Z}_1 + U\alpha]\int_0^{c_{SB}} S\,\mathrm{d}x_\beta - \rho_\infty\ddot{Z}_1\int_0^{c_{SB}} S[x_\beta - e_1]\,\mathrm{d}x_\beta - \rho_\infty\ddot{\beta}\int_0^{c_{SB}} S[x_\beta - e_1]^2\,\mathrm{d}x_\beta + M_g^\beta, \tag{30}$$

where the gust aerodynamics are

$$F_g^\beta = -\rho_\infty U\int_0^{c_{SB}} \frac{\mathrm{d}S}{\mathrm{d}x_\beta} w_g\,\mathrm{d}x_\beta + \rho_\infty\int_0^{c_{SB}} S\frac{Dw_g}{Dt}\,\mathrm{d}x_\beta \tag{31}$$

and

$$M_g^\beta = -\rho_\infty U\int_0^{c_{SB}} \frac{\mathrm{d}S}{\mathrm{d}x_\beta} w_g(x_\beta - e_1)\,\mathrm{d}x_\beta + \rho_\infty\int_0^{c_{SB}} S\frac{Dw_g}{Dt}(x_\beta - e_1)\,\mathrm{d}x_\beta. \tag{32}$$

As shown in Eqs. (31) and (32), the gust aerodynamic load acting on the store depends upon the gust wavelength over the store chord.

2.3. Aeroelastic state-space equations

Consider a discrete time history of the delta wing, $q(t)$, and the store, $\beta(t)$, with a constant sampling time step, Δt. The structural dynamic equations (15)–(17), can be reconstituted as a state-space equation in discrete time form as

$$[D_2]\{\theta\}^{t+1} + [D_1]\{\theta\}^t + [C_2]\{\Gamma\}^{t+1} + [C_1]\{\Gamma\}^t = -\{F_N^p\}^{t+1/2} + \{F_N^\beta\}^{t+1/2} + \{F^G(w_g)\}^{t+1}, \tag{33}$$

where the vector $\{\theta\}$ is the state of the plate, $\{\theta\} = \{\dot{q}, \dot{\beta}, q, \beta\}$ and $[D_1], [D_2]$ are matrices describing the wing plate and store structural behavior. $[C_1], [C_2]$ are matrices describing the vortex element behavior on the delta wing itself. $\{F_N^p\}$ and $\{F_N^\beta\}$ are the nonlinear force matrices generated by the wing plate structural nonlinearity and the freeplay junction between the wing and store, respectively. $\{F^G(w_g)\}$ are the gust aerodynamic generalized forces.

There is a linear relationship between the downwash w at the collocation points and delta wing response, $\{\theta\}$. It is defined by

$$\{w\} = [E]\{\theta\}. \tag{34}$$

In addition, of course, there is a downwash due to the gust given by Eqs. (22) (for the delta wing) and (27) (for the store). Thus, we obtain a complete aeroelastic state-space equation in matrix form:

$$\begin{bmatrix} A & -E \\ C_2 & D_2 \end{bmatrix} \begin{Bmatrix} \Gamma \\ \theta \end{Bmatrix}^{t+1} + \begin{bmatrix} B & 0 \\ C_1 & D_1 \end{bmatrix} \begin{Bmatrix} \Gamma \\ \theta \end{Bmatrix}^{t} = \begin{Bmatrix} 0 \\ (-F_N^p + F_N^\beta)^{t+1/2} \end{Bmatrix} + \begin{Bmatrix} w_g^{t+1} \\ F^G(w_g^{t+1/2}) \end{Bmatrix}. \tag{35}$$

3. Reduced order aerodynamic model

If we assume the structural response to be zero and no gust excitation, then from Eq. (23) one obtains a representation of the unforced fluid motion,

$$A\Gamma^{t+1} + B\Gamma^t = 0. \tag{36}$$

From Eq. (36), an aerodynamic eigenvalue problem may be formed. Since the matrices A and B are nonsymmetric, we must compute the right and left eigenvalues and eigenvectors of the generalized eigenvalue problem.

Let X and Y be the right and left eigenvector matrices, and Z is a diagonal matrix whose diagonal entries contain the eigenvalues. The right and left eigenvectors are orthogonal with respect to the matrices, A and B. We normalize the eigenvectors such that they are orthonormal with respect to A.

The vortex lattice aerodynamic model may be "reduced" using aerodynamic eigenmodes [23]. To accomplish this a transformation from the original flow variables $\{\Gamma\}$ to the modal variables $\{\gamma\}$ is made

$$\Gamma = X_{R_a}\gamma,$$

where γ is the vector of the aerodynamic modal coordinates. Γ, be a linear combination of the R_a right eigenvectors (where usually in practice $R_a \ll$ total number of aerodynamic eigenvalues). To account for the neglected eigenmodes therefore, we use a quasi-static correction which accounts for much of their influence. Let

$$\Gamma = \Gamma_s + \Gamma_d = \Gamma_s + X_{R_a}\gamma_d,$$

where the first term on the right-hand side is a quasi-static solution of the vortex flow and the second term is a dynamic perturbation solution. By definition, the quasi-static portion Γ_s is given by

$$[A + B]\Gamma_s^t = w^t + w_g^t, \tag{37}$$

where w^t and w_g^t are the downwashes at time step t. Compare Eqs. (22) and (37). Note that Eq. (37) may be inverted once to determine Γ_s^t in terms of $w^t + w_g^t$ and does *not* need to be evaluated at each time step.

The reduced order model with static correction is thus given by

$$\begin{bmatrix} I & -Y_{R_a}^T[I-A(A+B)^{-1}]E \\ C_2X_{R_a} & D_2+C_2(A+B)^{-1}E \end{bmatrix} \begin{Bmatrix} \gamma_d \\ \theta \end{Bmatrix}^{t+1} + \begin{bmatrix} -Z_{R_a} & +Y_{R_a}^T B(A+B)^{-1}E \\ C_1X_{R_a} & D_1+C_1(A+B)^{-1}E \end{bmatrix} \begin{Bmatrix} \gamma_d \\ \theta \end{Bmatrix}^{t}$$
$$= \begin{Bmatrix} 0 \\ -F_N+F_N^{\beta}+F^G(w_g) \end{Bmatrix}^{t+1/2} + \begin{bmatrix} Y_{R_a}^T[I-A(A+B)^{-1}] \\ -C_2(A+B)^{-1} \end{bmatrix} \{w_g\}^{t+1} + \begin{bmatrix} -Y_{R_a}^T B(A+B)^{-1} \\ -C_1(A+B)^{-1} \end{bmatrix} \{w_g\}^{t}. \quad (38)$$

4. Numerical results

The theoretical model is a simple delta wing configuration with a leading edge sweep of 45° and constructed from a 0.147-cm-thick plastic (Lucite). The root chord is partially clamped (cantilevered) and the length of the clamped portion of the root is 22.86 cm (60% root chord). The clamping is symmetric about the center of the root chord of the model. The length of the root chord is 38.1 cm. We use the aerodynamic vortex lattice model including 120 vortex elements on the delta wing ($km = kn = 15$) and 525 vortex elements in the wake ($kmm = 50$) and nine reduced aerodynamic eigenmodes $R_a = 9$. The delta wing structural modal numbers are $nxy = 10$ in the out-of-plane and $mxy = 200$ in the in-plane directions, respectively. The mesh of the finite-element model for the out-of- and in-plane structural model is 30×30 and thus the delta wing is modeled using 900 quadrilateral plate elements. The nodes at the clamped root chord satisfy geometric boundary conditions, i.e. $w = u = v = \theta_x = \theta_y = \theta_z = 0$. The first five natural frequencies of the delta wing plate alone are 4.39, 17.84, 20.62, 42.21 and 51.87 Hz. These results are obtained from a finite-element method using a standard code, ANSYS. The corresponding experimental results are discussed in Section 5.

The store is a slender body attached at the fore and aft support points of the delta wing. The slender body is a plastic tube, 1.59 cm in outside diameter and 13.6 cm in length. A paraboloidal forebody with 2.54 cm length is fixed to the fore end of the tube. The geometry of the paraboloidal forebody is described as

$$R/R_0 = \overline{x}_{\mathrm{SB}}^2, \quad \overline{x}_{\mathrm{SB}} = 0 \longrightarrow 1.$$

The slender body is symmetrical. The distance between the fore and aft attachment points is $e_2 = 10$ cm. $J_\beta = 0.4108E^{-4}\,\mathrm{N\,m\,s^2}$, $k_s = 35.8\,\mathrm{N/m}$. As shown in Fig. 1, $e_1 = 12.7$ cm, $e_3 = -2.1$ cm. $M_1 = 0.033$ kg, $M_2 = 0.0055$ kg. As shown in Eqs. (29) and (30), $\int_0^{c_{\mathrm{SB}}} S\,\mathrm{d}x_\beta = 3.045E^{-5}\,\mathrm{m^3}$, $\int_0^{c_{\mathrm{SB}}} S[x_\beta - e_1]\,\mathrm{d}x_\beta = 4.58E^{-7}\,\mathrm{m^4}$ and $\int_0^{c_{\mathrm{SB}}} S[x_\beta - e_1]^2\,\mathrm{d}x_\beta = 7.657E^{-8}\,\mathrm{m^5}$.

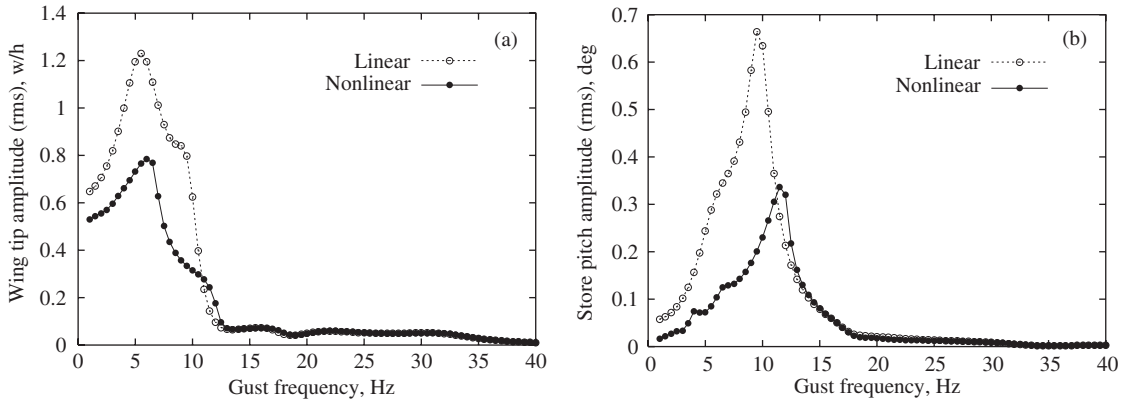

Fig. 2. Linear and nonlinear gust frequency responses for $U = 20$ m/s and gust angle amplitude of $\alpha_{g0} = 0.1°$: (a) wing tip frequency response, (b) store pitch frequency response; dashed line with ○, linear; solid line with ●, nonlinear.

4.1. Response to a periodic gust without freeplay

The theoretical lateral gust velocity amplitude is assumed to be $w_{g0} = \frac{0.1}{57.3} \times U$ or $\alpha_{g0} = 0.1^\circ$ for the basic case of a single harmonic gust load, see Eq. (20). Firstly, zero freeplay gap of the store is considered. Fig. 2 shows typical rms amplitude of the nondimensional wing tip response (Fig. 2(a)) and the store pitch response (Fig. 2(b)) vs. the gust frequency for the flow velocity, $U = 20\,\text{m/s}$ and gust angle amplitude, $\alpha_{g0} = 0.1^\circ$. To illustrate and contrast the effects of the wing structural nonlinearity on the gust response, the linear results are also plotted on this figure. As shown in Fig. 2(a) for the nondimensional wing tip response, there is a dominant peak rms amplitude at the gust frequency of 5.5 Hz for the linear system and 6.2 Hz for the nonlinear system. The wing structural nonlinearity leads to a higher structural stiffness. Thus, the response amplitude decreases and the peak frequency increases when structural nonlinearities are included in the theoretical analysis. In the higher gust frequency range ($\omega_g > 12\,\text{Hz}$), the response amplitude is smaller and the linear and nonlinear results are the same. As shown in Fig. 2(b), the dominant peak frequency for the store pitch response is 11.5 Hz for the nonlinear system and 9.5 Hz for the linear system. The dominant peak frequency for the wing tip and the store pitch responses is different, because the wing tip response is very sensitive to the bending modes (first bending mode for this case) and the store pitch response is sensitive to the dominant store pitch mode.

Fig. 3 shows rms amplitude of the nondimensional wing tip response (Fig. 3(a)) and the store pitch response (Fig. 3(b)) vs. the gust frequency for the several flow velocities, $U = 10$, 20 and 28 m/s and a gust angle

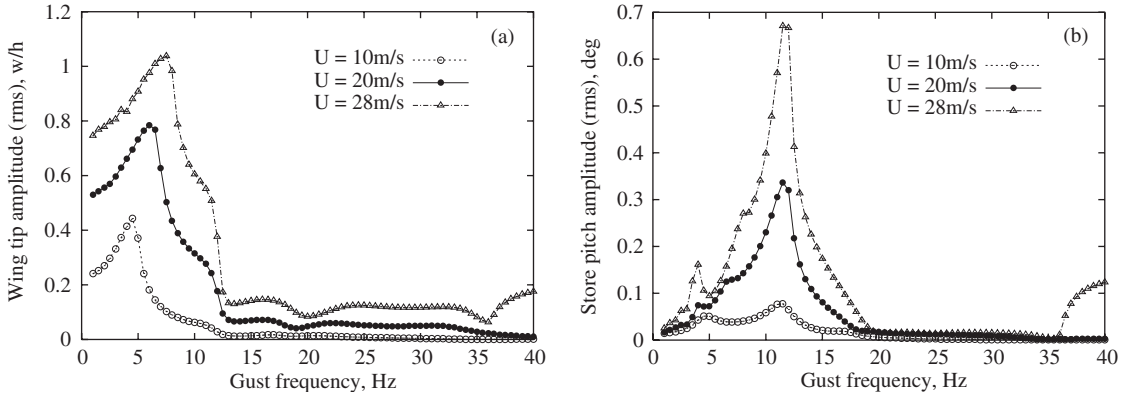

Fig. 3. Gust frequency response for a gust angle amplitude of $\alpha_{g0} = 0.1^\circ$ and several flow velocities: (a) wing tip frequency response, (b) store pitch frequency response; dashed line with ○, $U = 10\,\text{m/s}$; solid line with •, $U = 20\,\text{m/s}$; dashed point line with △, $U = 28\,\text{m/s}$.

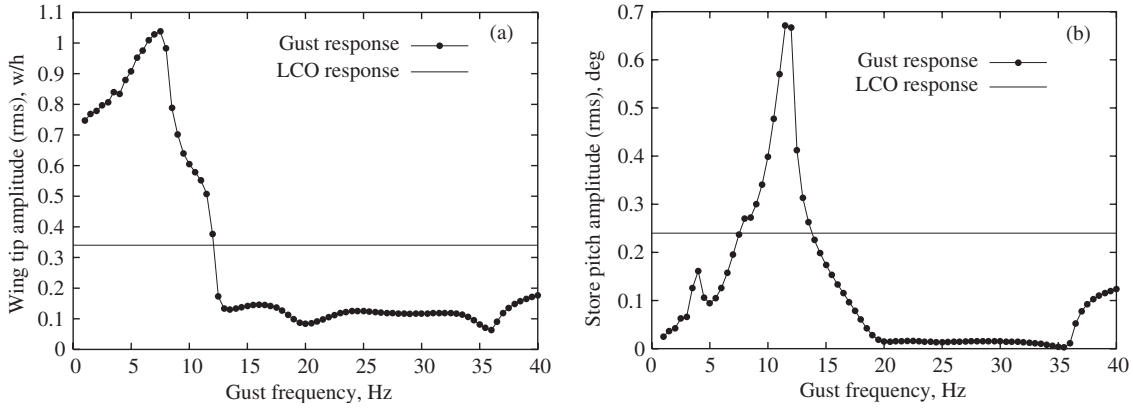

Fig. 4. Gust frequency response for a gust angle amplitude of $\alpha_{g0} = 0.1^\circ$ and a flow velocity of $U = 28\,\text{m/s}$: (a) wing tip frequency response, (b) store pitch frequency response; solid line with •, gust response; solid line, LCO response.

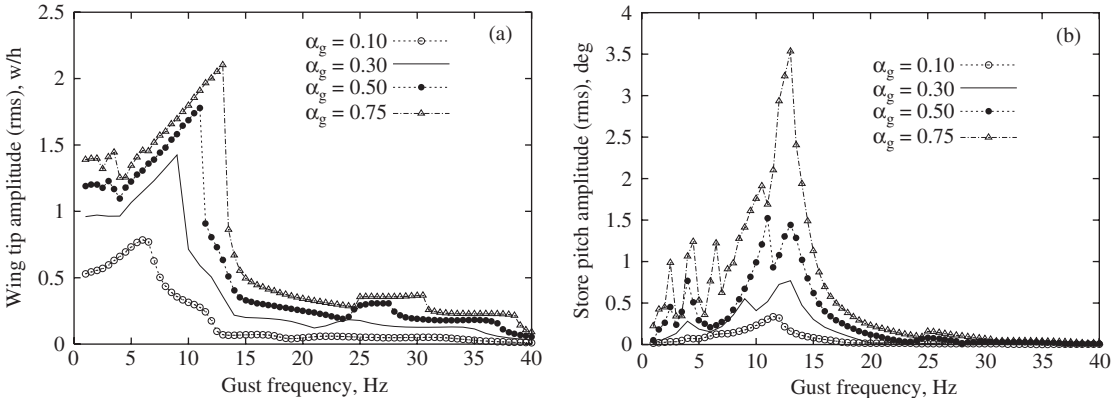

Fig. 5. Gust frequency response for a flow velocity of $U = 20\,\text{m/s}$ and several gust angle amplitudes: (a) wing tip frequency response, (b) store pitch frequency response; dashed line with ○, $\alpha_g = 0.1°$; dashed line with •, $\alpha_g = 0.3°$; solid line, $\alpha = 0.5°$; dashed point line with △, $\alpha = 0.75°$.

amplitude, $\alpha_{g0} = 0.1°$. Note that the linear flutter velocity is 24.5 m/s. Three points are of interest. First of all, for the wing tip response as shown in Fig. 3(a), the frequency corresponding to the peak amplitude increases as the flow velocity increases, i.e. growing from 4.5, 6.2 to 7.5 Hz when the flow velocity increases from 10, 20, to 28 m/s. This is expected due to the increase of the aerodynamic stiffness with increasing flow velocity and the wing geometrical nonlinearity. Secondly, for the store pitch response as shown in Fig. 3(b) the peak frequency is almost independent of the flow velocity, i.e. 11.5 Hz. This means that the resonant frequency dominated by the store pitch mode is not sensitive to the flow velocity. Thirdly, there is a rapid decreases in wing tip response at a gust frequency of 12.5 Hz for the flow velocity that is higher than the flutter velocity. Recall the flutter frequency is 9 Hz. It is interesting to find that the wing tip and the store pitch responses beyond 12.5 Hz are lower than the LCO amplitude when no gust load is present as shown in Figs. 4(a) and (b).

Fig. 5 shows rms amplitude of the nondimensional wing tip response (Fig. 5(a)) and the store pitch response (Fig. 5(b)) vs. the gust frequency for the flow velocity, $U = 20\,\text{m/s}$ and several gust angle amplitudes. For the wing tip response as shown in Fig. 5(a), the frequency corresponding to the peak amplitude increases as the gust angle amplitude increases, i.e. growing from 6.2, 9, 11 to 13 Hz when the gust angle amplitude increases from 0.1°, 0.3°, 0.5° to 0.75°. This is because the effect of the wing geometrical nonlinearity on the first wing natural bending mode becomes stronger when the aerodynamic forces increase. For the store pitch response as shown in Fig. 5(b) the peak frequency increases from 11.5 to 13 Hz as the gust angle amplitude increases. Also it is interesting to note that there are some rapid changes in responses at the peak response frequencies for the higher gust angle amplitudes for the wing tip response.

Figs. 6(a) and (b) show typical time histories of the nondimensional wing tip response (Fig. 6(a)) and the store pitch response (Fig. 6(b)) for the flow velocity, $U = 28\,\text{m/s}$, $\alpha_{g0} = 0.1°$ and gust frequency 5 Hz. Both the wing tip and store pitch responses are periodic motions. Fig. 6(c) shows the FFT analysis corresponding to Figs. 6(a) and (b). The dominant peak frequency is 5 Hz and the response at 15 Hz is most important for the store pitch motion (dominant store pitch mode). The response at 25 Hz corresponds to the second bending mode of this system.

4.2. Response to a periodic gust with freeplay

Now both the store freeplay nonlinearity and the wing geometric structural nonlinearity of the wing–store model are considered. Two freeplay gap values, $d = \delta/h = 0.5$, 1.0 are chosen for the calculations.

Fig. 7 shows rms amplitude of the nondimensional wing tip response (Fig. 7(a)) and the store pitch response (Fig. 7(b)) vs. the gust frequency for several flow velocities, $U = 10$, 20 and 28 m/s and gust angle amplitude, $\alpha_{g0} = 0.1°$ and freeplay, $d = 0.5$. When we compare Fig. 7 to 3 for $d = 0$, it is interesting to find the response behavior in the frequency range of 1–12.5 Hz is very similar for the wing tip motions. In the higher frequency

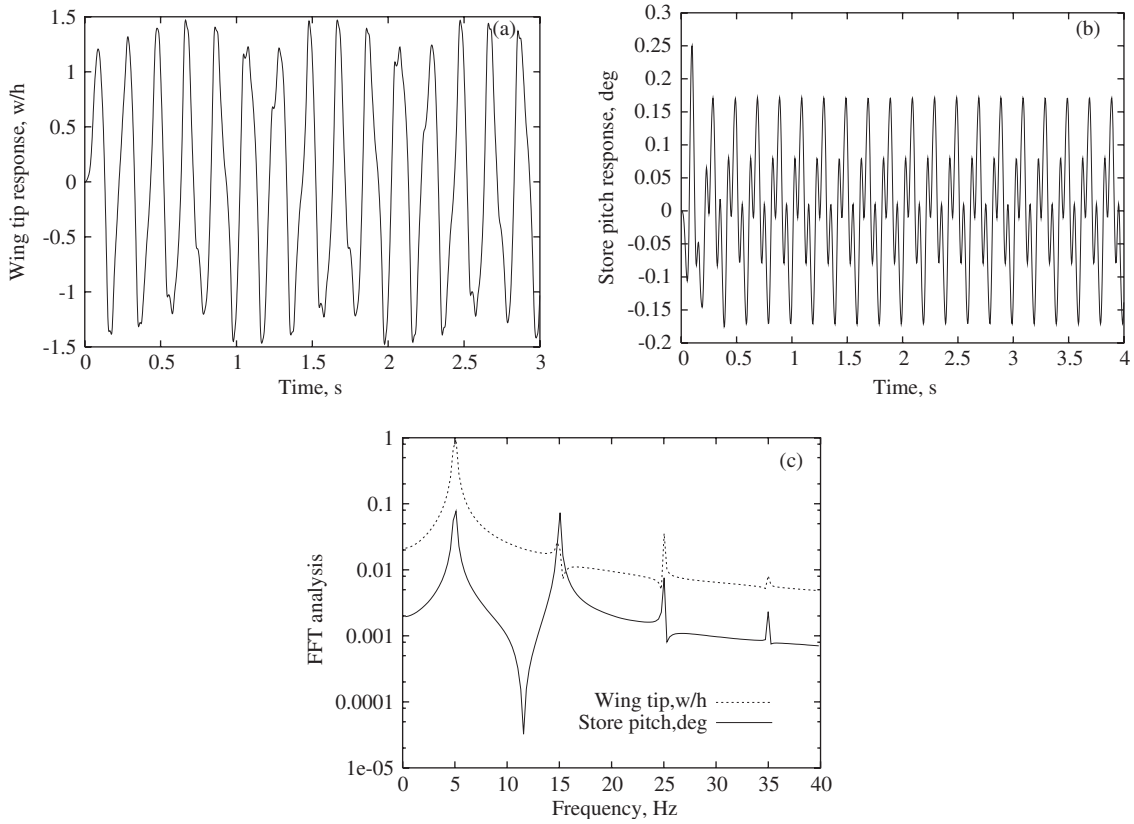

Fig. 6. Time histories and FFT analysis for the wing tip and store pitch responses for a flow velocity of $U = 28\,\mathrm{m/s}$, $\alpha_{g0} = 0.1^\circ$ and a gust frequency of 5 Hz: (a) wing tip frequency response, (b) store pitch frequency response, (c) FFT analysis; solid line, store pitch response (deg); dashed line, wing tip response (w/h).

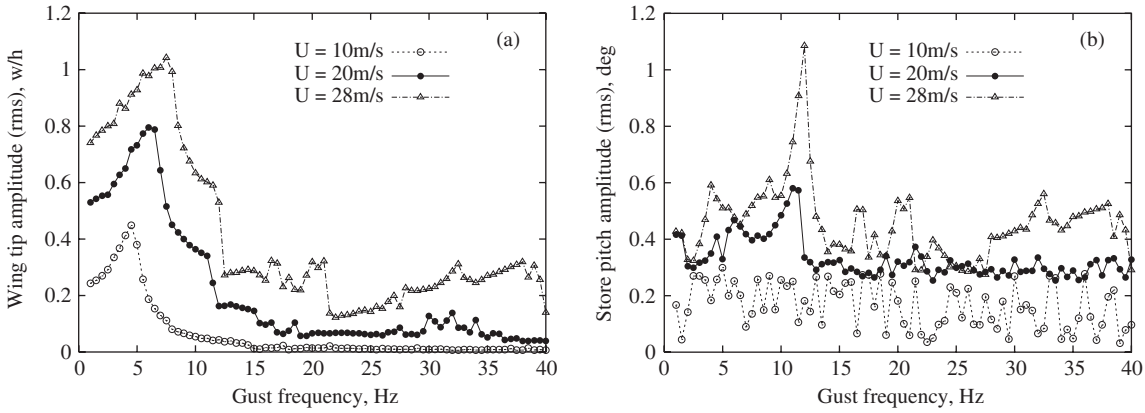

Fig. 7. Gust frequency response for a gust angle amplitude of $\alpha_{g0} = 0.1^\circ$, $d = 0.5$ and several flow velocities: (a) wing tip frequency response, (b) store pitch frequency response; dashed line with ○, $U = 10\,\mathrm{m/s}$; solid line with •, $U = 20\,\mathrm{m/s}$; dashed point line with △, $U = 28\,\mathrm{m/s}$.

range, the wing tip amplitude becomes larger as the flow velocity increases and the frequency response is more complex with freeplay than without. For the store pitch response, Fig. 7(b) for $d = 0.5$ and Fig. 3(b) for $d = 0$ are entirely different. The frequency response curve becomes very irregular with freeplay. This is because the

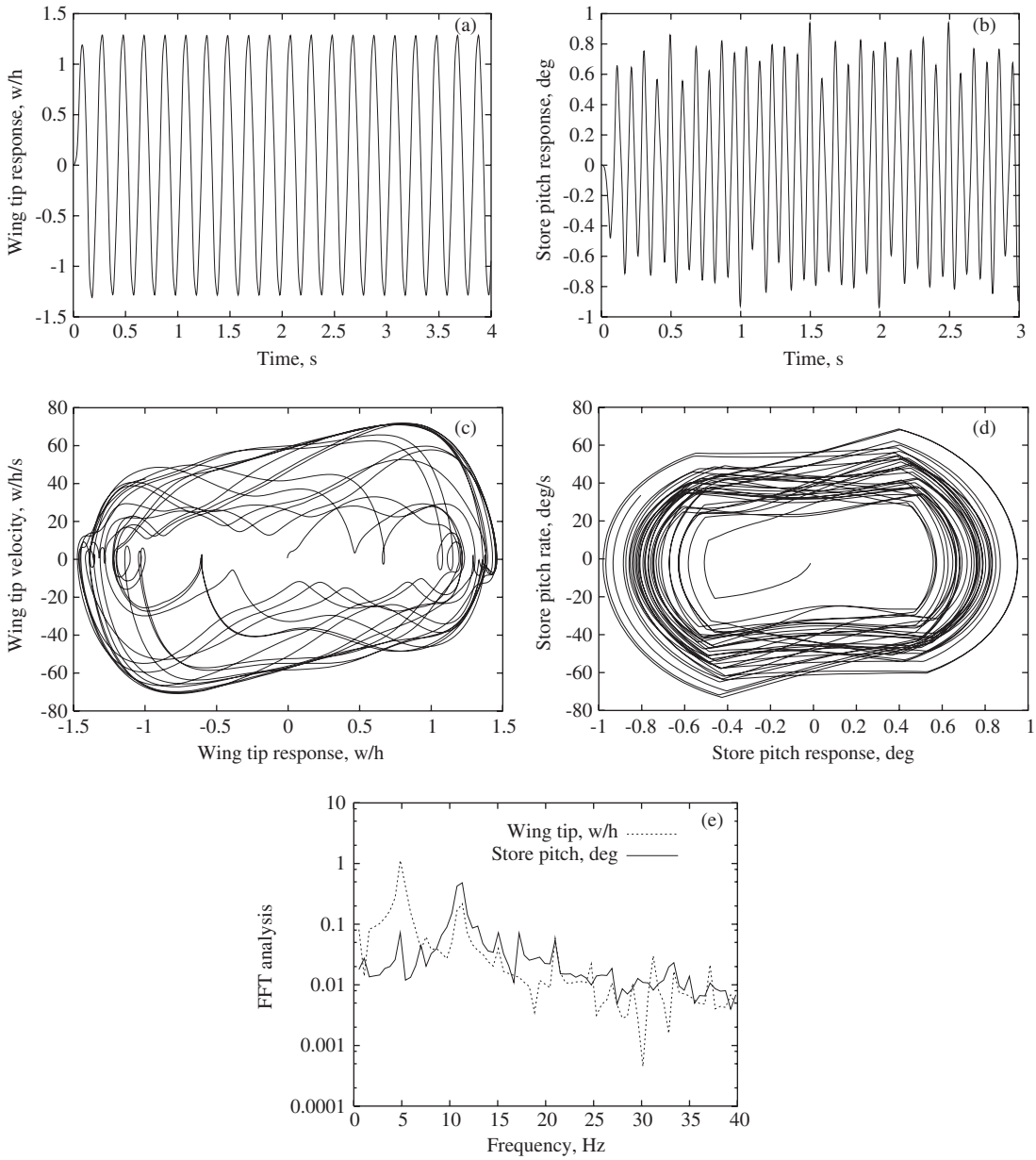

Fig. 8. Wing tip and store pitch response for $U = 28\,\mathrm{m/s}$, $\alpha_{g0} = 0.1^\circ$, $d = 0.5$ and $\omega_g = 5\,\mathrm{Hz}$: (a) wing tip response, (b) store pitch response, (c) $\dot{w}/h$ vs. w/h, (d) $\dot{\beta}$ vs. β, (e) FFT analysis; solid line, store pitch response (deg); dashed line, wing tip response (w/h).

wing tip and store pitch motions become nonperiodic or chaotic with freeplay ($d = 0.5$) rather than the periodic motions without freeplay ($d = 0$). For an explanation of this phenomenon, a set of figures for a typical example, $U = 28\,\mathrm{m/s}$, $\alpha_{g0} = 0.1^\circ$, gust frequency 5 Hz and $d = 0.5$ are shown in Fig. 8. Note that this example is the same as Fig. 6, but $d \neq 0$.

Figs. 8(a) and (b) show the time histories of the nondimensional wing tip response (Fig. 8(a)) and the store pitch response (Fig. 8(b)). Comparing Fig. 8(a) for $d = 0.5$ to 6(a) for $d = 0$, the rms wing tip amplitudes are almost identical but the motion time history is different. Comparing Fig. 8(b) to 6(b), both the store pitch amplitudes and motion behavior are entirely different. Figs. 8(c) and (d) show the phase plane plots of w/h vs. $\dot{w}/h$ and β vs. $\dot{\beta}$. There are two rest points (equilibrium positions) for the pitch motion, i.e. -0.43° and $+0.43^\circ$. The response motion is nonperiodic around the two rest points. The FFT analysis of the wing tip and the store

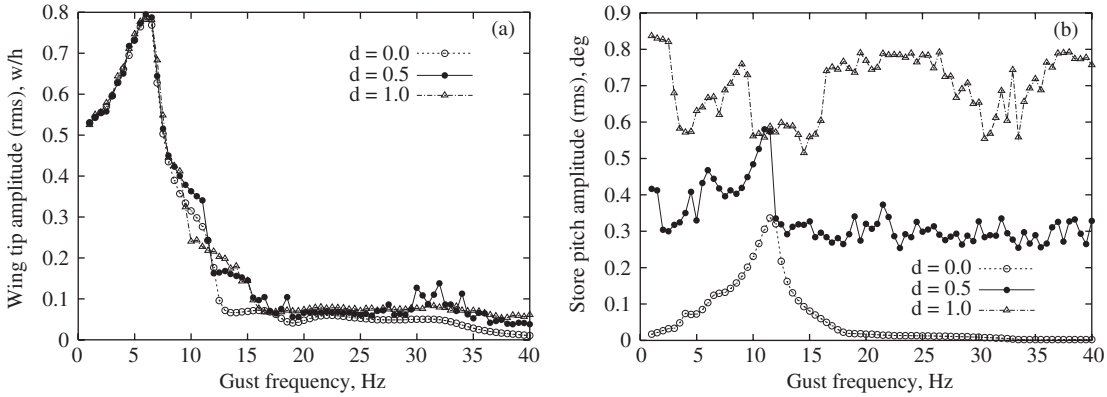

Fig. 9. Gust frequency response for a gust angle amplitude of $\alpha_{g0} = 0.1^\circ$, $U = 20\,\text{m/s}$ and several freeplay gap values: (a) wing tip frequency response, (b) store pitch frequency response; dashed line with ○, $d = 0$; solid line with •, $d = 0.5$; dashed point line with △, $d = 1.0$.

pitch motions is shown in Fig. 8(e) (note the logarithmic scale). There is a dominant harmonic peak component (at 5 Hz) and also higher harmonic components for the wing tip motion. For the store pitch motion the dominant harmonic peak component is at 11 Hz but there is a complex response overall. Comparing Fig. 8(e) to 6(c), a very significant difference is observed.

Now consider the effects of the freeplay gap on the gust response. Two typical flow velocities, $U = 20$ and 28 m/s are used in the calculations. For the flow velocity lower than the flutter, $U = 20\,\text{m/s}$, the results are shown in Figs. 9(a) and (b) for the wing tip and the store pitch responses. Although there is a significant difference in the store pitch response, the change in the wing tip response due to the freeplay gap is small. However, as shown in Ref. [18] for the same wing/store model, the LCO (no gust) amplitude of the wing tip response is significantly dependent on the store pitch response and the freeplay gap.

Figs. 10(a) and (b) show the time histories of the wing tip response (Fig. 10(a)) and the store pitch response (Fig. 10(b)) for $u = 20\,\text{m/s}$, $d = 0.5$ and $\omega_g = 25\,\text{Hz}$. A chaotic response for both the wing tip and the store motion is found. Figs. 10(c) and (d) show the phase plane plots of w/h vs. $\dot{w}/h$ and β vs. $\dot{\beta}$. The response motion is nonperiodic around the two rest points, $\beta = -0.43^\circ$ and $+0.43^\circ$. The FFT analysis of the store pitch motions is shown in Fig. 10(e). There is a relatively broad frequency band width with a dominant harmonic peak component at 25 Hz.

For a flow velocity higher than the flutter velocity, results are shown in Figs. 11(a) and (b) for $U = 28\,\text{m/s}$. As shown in Fig. 11(a) for the wing tip response, there is a rapid decrease in response beyond a frequency of 12.5 Hz which is similar to that of Fig. 4(a) for the model without freeplay. However, the response amplitude beyond this frequency is higher than the no gust response amplitude (LCO) and this is different from the result shown in Fig. 4 for the case of no freeplay.

The effects of gust angle amplitude on the gust response are considered next. Fig. 12 shows rms amplitude of the nondimensional wing tip response (Fig. 12(a)) and the store pitch response (Fig. 12(b)) vs. the gust frequency for the flow velocity, $U = 20$, $d = 1.0$ and several gust angle amplitudes. For the wing tip response as shown in Fig. 12(a), the frequency corresponding to the peak amplitude increases as the gust angle amplitude increases, i.e. growing from 6.2, 9 to 11 when the gust angle amplitude increases from 0.1°, 0.3°, to 0.5°. The rapid change in response becomes clearer when the gust angle amplitude increases. For the store pitch response as shown in Fig. 12(b), the motion is complex and chaotic. The rms amplitude vs. gust frequency becomes very irregular.

As shown in Ref. [18], the effects of the initial conditions on the LCO (no gust amplitude) behavior can be important. Here for the gust response, three initial condition cases, I.C.1, I.C.2 and I.C.3, are used. For I.C.1, the nondimensional wing tip displacement is $w(0)/h = 0.001$ and the wing displacement at other points on the wing, the store pitch angle, $\beta(0)$, and the reduced vortex strength, $\gamma(0)$, are zero. For I.C.2, the initial store pitch angle, $\beta(0) = 0.5^\circ$ but all wing displacements and all initial velocities are zero. Note that the static

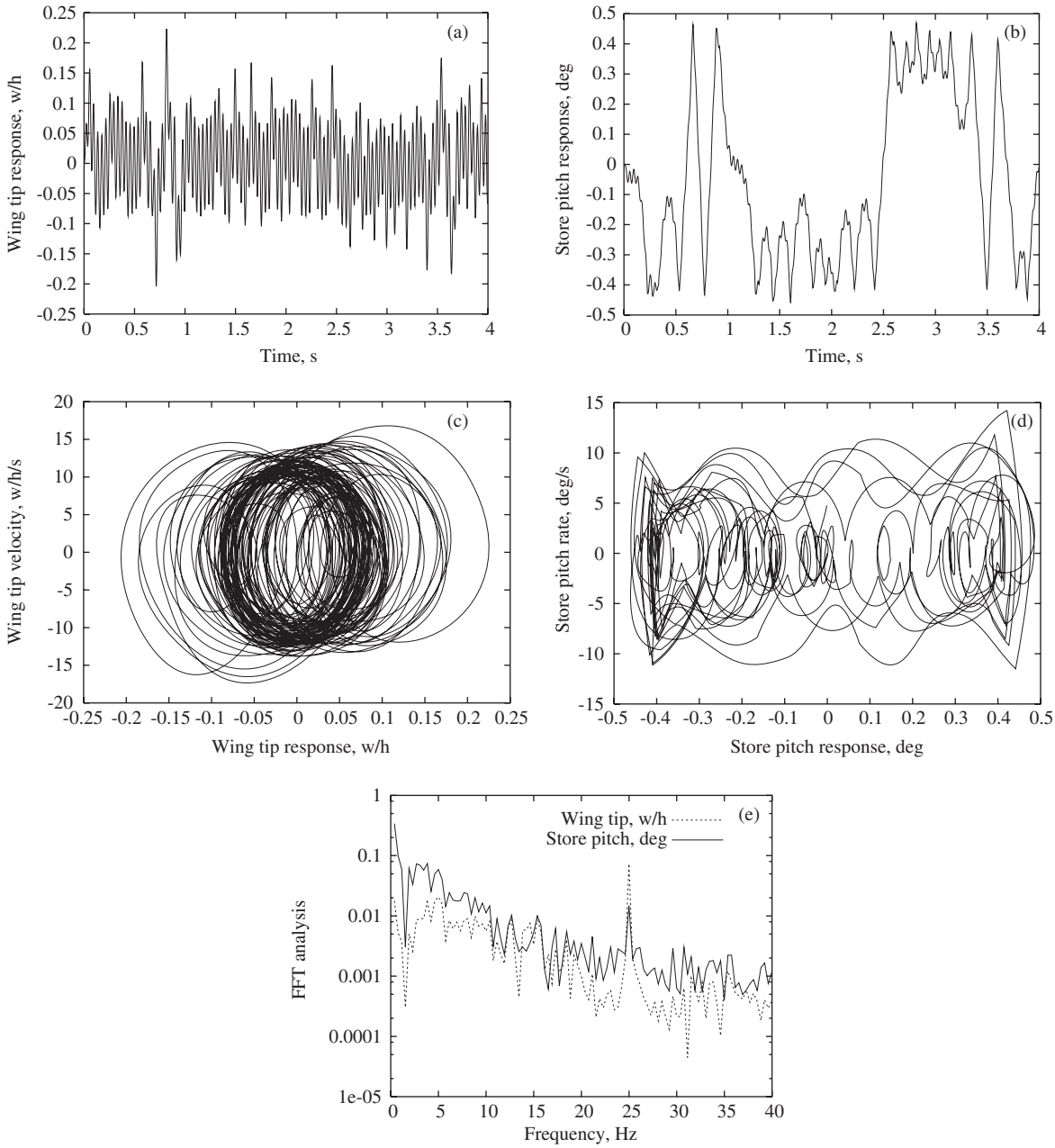

Fig. 10. Wing tip and store pitch response for $U = 20\,\mathrm{m/s}$, $d = 0.5$, $\alpha_{g0} = 0.1^\circ$ and $\omega_g = 25\,\mathrm{Hz}$: (a) wing tip response, (b) store pitch response, (c) $\dot{w}/h$ vs. w/h, (d) $\dot{\beta}$ vs. β, (e) FFT analysis; solid line, store pitch response (deg); dashed line, wing tip response (w/h).

equilibrium position of the store for $d = 0.5$ is 0.428°. For I.C.3, the initial store pitch angle $\beta(0) = 1.0^\circ$ but all wing displacements and all velocities are zero. Note that the static equilibrium position of the store for $d = 1.0$ is 0.856°. The effects of the initial conditions are shown in the following figures.

Fig. 13 shows rms amplitude of the nondimensional wing tip response (Fig. 13(a)) and the store pitch response (Fig. 13(b)) vs. the gust frequency for flow velocity, $U = 10\,\mathrm{m/s}$, the gust angle amplitude, $\alpha_{g0} = 0.1^\circ$, freeplay $d = 0.5$ and the several initial conditions. The effects of the initial conditions on the gust response are small for the smaller flow velocities.

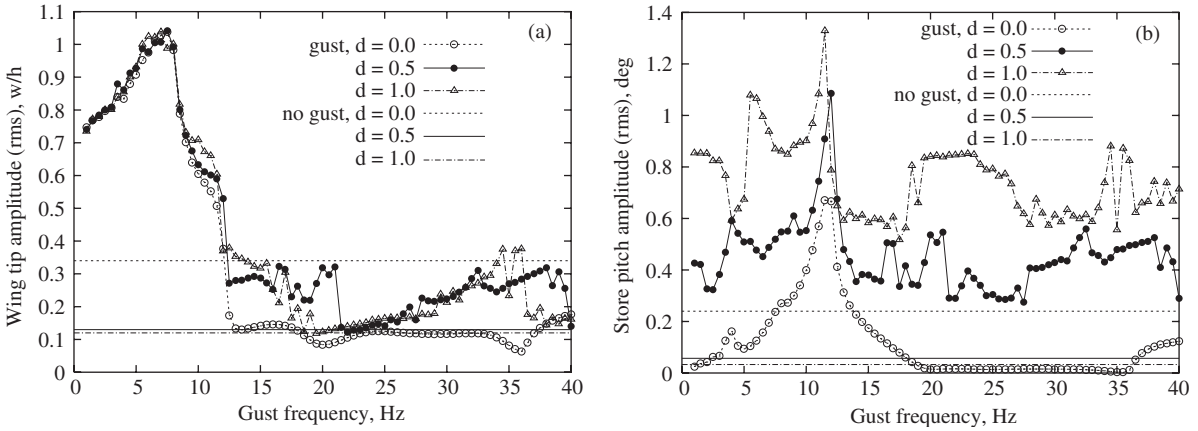

Fig. 11. Gust frequency response for a gust angle amplitude of $\alpha_{g0} = 0.1^\circ$, $U = 28\,\mathrm{m/s}$ and several freeplay gap values: (a) wing tip frequency response, (b) store pitch frequency response; dashed line with ○, gust response, $d = 0$; solid line with •, gust response, $d = 0.5$; dashed point line with △, gust response, $d = 1.0$; dashed line, no gust response, $d = 0$; solid line, no gust response, $d = 0.5$; dashed point line, no gust response, $d = 1.0$.

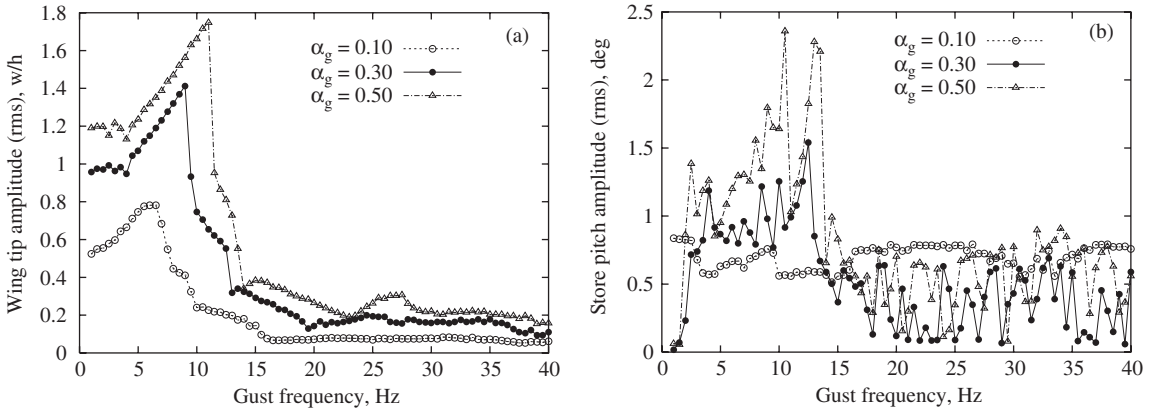

Fig. 12. Gust frequency response for a flow velocity of $U = 20\,\mathrm{m/s}$, $d = 1.0$ and several gust angle amplitude: (a) wing tip frequency response, (b) store pitch frequency response; dashed line with ○, $\alpha_g = 0.1^\circ$; solid line with •, $\alpha_g = 0.3^\circ$; dashed point line with △, $\alpha = 0.5^\circ$.

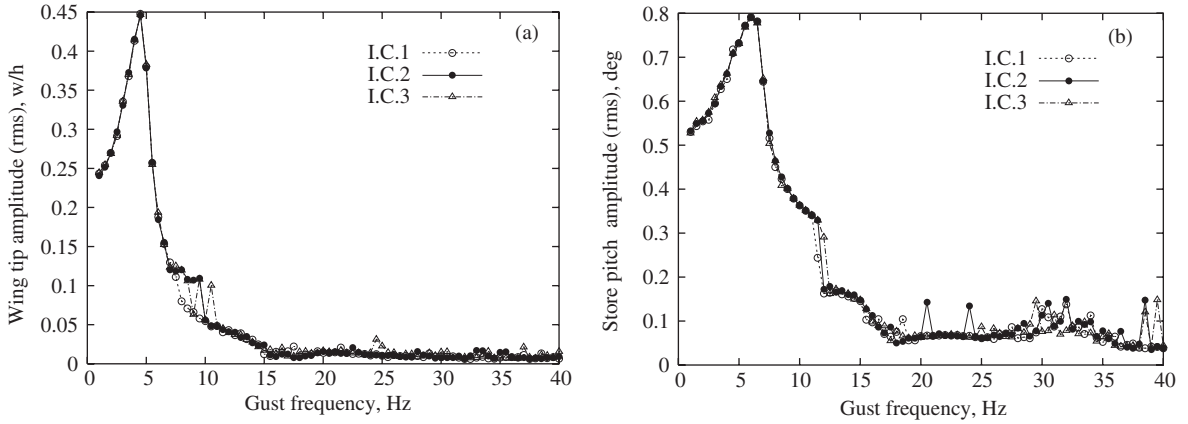

Fig. 13. Gust frequency response for a gust angle amplitude of $\alpha_{g0} = 0.1^\circ$, $U = 10\,\mathrm{m/s}$, $d = 0.5$ and several initial conditions: (a) wing tip frequency response, (b) store pitch frequency response; dashed line with ○, I.C.1; solid line with •, I.C.2; dashed point line with △, I.C.3.

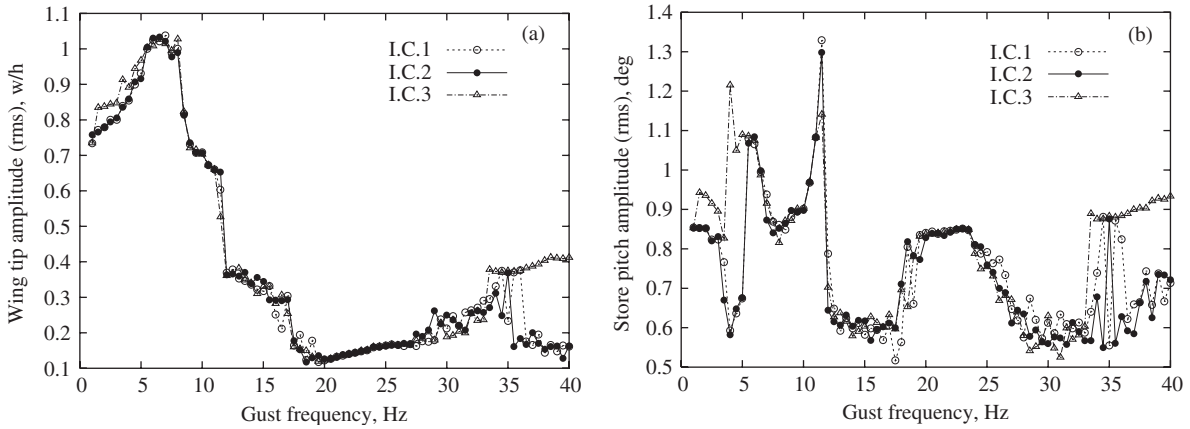

Fig. 14. Gust frequency response for gust angle amplitude, $\alpha_{g0} = 0.1^\circ$, $U = 28\,\mathrm{m/s}$, $d = 1.0$ and the several initial conditions: (a) wing tip frequency response, (b) store pitch frequency response; dashed line with ○, I.C.1; solid line with •, I.C.2; dashed point line with △, I.C.3.

Fig. 14 shows rms amplitude of the nondimensional wing tip response (Fig. 14(a)) and the store pitch response (Fig. 14(b)) vs. the gust frequency for flow velocity, $U = 28\,\mathrm{m/s}$, the gust angle amplitude, $\alpha_{g0} = 0.1^\circ$, freeplay $d = 1.0$ and the several initial conditions. The effects of the initial conditions on the gust response are still small except in the higher frequency range, $\omega_g > 33\,\mathrm{Hz}$.

5. Theoretical and experimental correlations

5.1. Experimental model

The experimental delta wing and the store configurations are the same as those of the theoretical model. The store pitch stiffness, k_s, is 35.77 N/m and corresponding store pitch natural frequency is 14.63 Hz. The first five natural frequencies of the delta wing plate alone are 4.39, 17.84, 20.62, 42.21 and 51.87 Hz. These results are obtained from a finite-element method using a standard code, ANSYS. The corresponding experimental results are 4.5, 17.2, 20.54, 44.4 and 54.4 Hz. A steel leaf-spring is inserted tightly into the store body near the fore support (articulated point).

The free end of the leaf-spring is attached to the aft support point with a certain freeplay gap value. Two strain gages are glued to both sides near the fixed end of the leaf-spring and are used to measure the store pitch angle. The dynamic calibration coefficient was determined by a ground vibration test.

The gust was created by placing a rotating slotted cylinder (RSC) behind an airfoil upstream of the delta wing model. The gust generator configuration in the wind tunnel had two airfoils or vanes and two rotating slotted cylinders. The distance between these vanes was 12″. For details of the gust generator design, see Ref. [7].

A micro-accelerometer is fixed on the wing mid-span of the trailing edge. The acceleration amplitude of the gust response is measured from this transducer. The calibration coefficient is $s_a = g/\mathrm{V}$, where g is the gravity acceleration, $g = 9.81\,\mathrm{m/s^2}$. A typical span location of the store for the "leading edge" case, $y/c = 0.68$ (near the wing tip), two freeplay gap values, $d = 0.5$ and 1.0, and three flow velocities, $U = 10$, 18.5 and 28 m/s are considered in the experiment. Note that the linear flutter velocity is 24.5 m/s. A data acquisition system, LabView 7.0 version, is used to obtain the measurement data. The sampling rate is 1000 points/s, $\Delta t = 1/1000$, and the total sampling length is 10 000 points. An ensemble averaged FFT analysis is used to determine the response frequency using a time delay average method. The delay time is $2 \times \Delta t$ and the FFT analysis uses 2048 sampling points. The ensemble average number is 100. A rms acceleration amplitude is used to represent the correlations between the theory and experiment. The experimental rms acceleration amplitude is obtained from the time history over 10 000 sampling points.

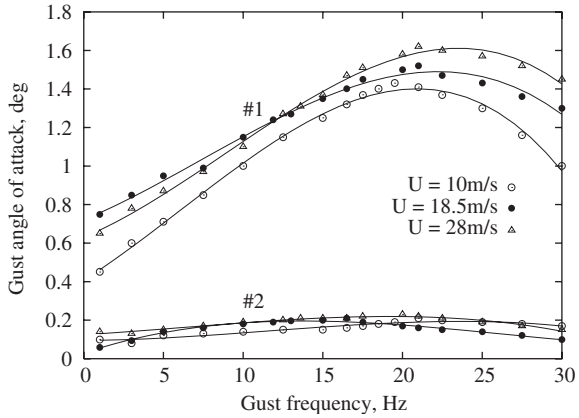

Fig. 15. Experimental gust angle of attack vs. gust frequency for $U = 10$, 18.5 and 28 m/s: ○, $U = 10$ m/s; •, $U = 18.5$ m/s; △, $U = 28$ m/s.

5.2. Gust field

In order to obtain a more meaningful correlation between theory and experiment, the gust field is measured and quantitatively calibrated before the wing–store model test. For details of the gust field measurement, see Ref. [7]. Fig. 15 shows the measured gust angle of attack, α_g vs. gust excitation frequency, Hz, for the flow velocities of $U = 10$, 18.5 and 28 m/s which are considered in the following theoretical and experimental analysis. In this figure, a symbol ○ indicates the measured first and second harmonic components for the flow velocity $U = 10$ m/s and the symbols • and △ indicate the measured values for $U = 18.5$ and 28 m/s, respectively. The solid lines are least-squares curve fittings of the experimental data. A formula based upon the measured experimental gust angle of attack is constructed as

$$\alpha_g(t) = \alpha_{g1} \sin \omega_g t + \alpha_{g2} \sin(2\omega_g t + \Delta\phi). \tag{39}$$

Eq. (39) is used as an gust excitation to calculate the nonlinear gust response for comparison with the experimental results where α_{g1} and α_{g2} are the first and second gust amplitude of the gust excitation. $\Delta\phi$ is a phase difference between first and second gust frequencies. It is difficult to measure this phase angle for the present RSC gust generator. Here, we assume $\Delta\phi = 0$ as an approximation.

Typical gust time histories and corresponding FFT analysis for several flow velocities and gust frequencies corresponding to the data in Fig. 15 are shown in Figs. 18(a)–(c) and corresponding FFT plots in Figs. 17(f), 20(f) and 23(f).

5.3. Gust response

Fig. 16(a) shows the acceleration frequency response curves at the wing mid-span of the trailing edge for flow velocity $U = 10$ m/s. The theoretical results are shown by a solid line for no freeplay gap ($d = 0$), a broken line for $d = 0.5$ and a dashed line for $d = 1.0$ that are based on the experimental gust angle vs. the gust frequency curve of $U = 10$ m/s as shown in Fig. 15, and also for Fig. 19 ($U = 18.5$ m/s) and Fig. 22 ($U = 28$ m/s). The experimental results are shown by a symbol of ○ for no freeplay gap ($d = 0$), a symbol of • for $d = 0.5$ and a symbol of △ for $d = 1.0$. Note that in Fig. 16, the measured response is not a pure harmonic motion, therefore we use an average rms method to characterize the response for correlation purposes. The store pitch angle frequency response curves corresponding to Fig. 16(a) are shown in (b). For the measured store pitch response, the store pitch angle scaling is calibrated by the linear system, i.e. for no freeplay. With freeplay, this scale is not precisely accurate because in the freeplay range, the strain of the leaf-spring is zero. The error is at least 0.428° for $d = 0.5$ and 0.856° for $d = 1$. Thus we did not include the experimental data for $d = 0.5$ and 1.0 in this figure.

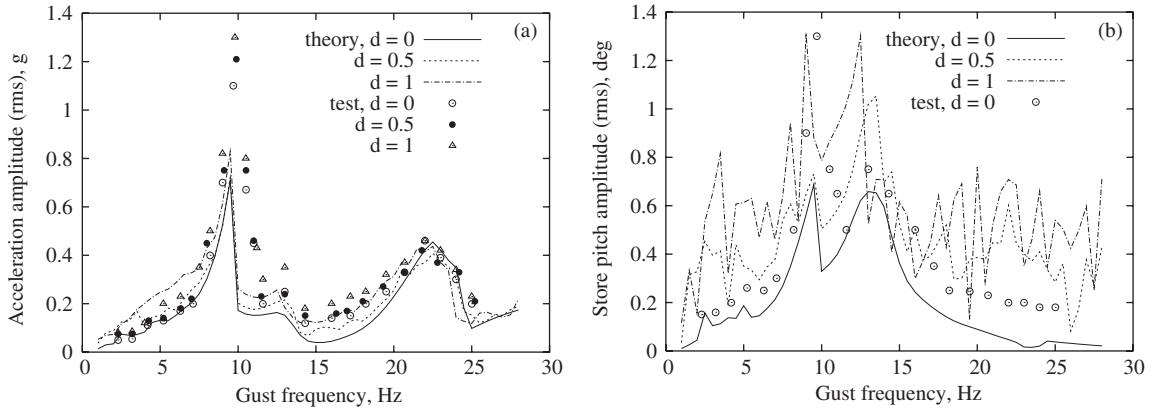

Fig. 16. Theoretical and experimental gust frequency response for $U = 10\,\mathrm{m/s}$, and the several freeplay gaps, $d = 0$, 0.5 and 1: (a) wing tip frequency response, (b) store pitch frequency response; ○, test, $d = 0$; •, test, $d = 0.5$; △, test, $d = 1.0$; solid line, theory, $d = 0$; dashed line, theory, $d = 0.5$; dashed point line, theory, $d = 1.0$.

For Fig. 16(a), there are three peak amplitudes near the gust frequencies, $\omega_g = 9.8$, 12.5 and 22 Hz. The dominant peak amplitude is near $\omega_g = 9.8\,\mathrm{Hz}$ which corresponds to the first bending mode of the aeroelastic system. For the store pitch response, there is a peak amplitude near $\omega_g = 14.5\,\mathrm{Hz}$ which is dominated by the first torsional mode of the aeroelastic system. The quantitative agreement between the theory and experiment is reasonably good except near the resonant frequency, $\omega_g = 9.8$–$10.5\,\mathrm{Hz}$.

Figs. 17(a) and (b) show the typical measured time responses of the wing acceleration (a), the store pitch angle (b) for $U = 10\,\mathrm{m/s}$, $\omega_g = 19.5\,\mathrm{Hz}$ and no freeplay gap ($d = 0$). As shown in Fig. 17(a), there is a "beat" phenomenon. This is because of the unsteady gust load as shown in the gust time history of Fig. 18(a). The theoretical time responses corresponding to Figs. 17(a) and (b) are shown in Figs. 17(c) and (d). The corresponding theoretical and experimental FFT analysis is shown in Figs. 17(e) and (f). The dominant frequency response component is located at the frequency, $\omega_g = 19.5\,\mathrm{Hz}$ and there is a detectable $2\omega_g$ frequency components in addition to a dominant ω_g component for this measured nonlinear system. There is a noise in the measured signals for both Figs. 17(e) and (f). This is because the gust field is unsteady. In order to observe the relationship between the wing/store model dynamic response and the gust excitation, the measured gust flow field (gust angle time history) for $U = 10\,\mathrm{m/s}$ and $\omega_g = 19.5\,\mathrm{Hz}$ is shown in Fig. 18(a). The corresponding FFT analysis of the measured gust excitation is also plotted in Fig. 17(f). The dominant harmonic amplitude of the gust angle is $\alpha_{g1} = 1.43^\circ$ and the second harmonic gust amplitude is $\alpha_{g2} = 0.17^\circ$.

Fig. 19(a) shows the acceleration frequency response curves at the wing mid-span of the trailing edge for flow velocity $U = 18.5\,\mathrm{m/s}$. The store pitch angle frequency response curves corresponding to Fig. 19(a) are shown in Fig. 19(b). For Fig. 19(a), there are the very obvious peak amplitude near the gust frequency, $\omega_g = 14\,\mathrm{Hz}$ (theory) and $\omega_g = 14.7\,\mathrm{Hz}$ (experiment) and the second theoretical peak amplitude at $\omega_g = 28\,\mathrm{Hz}$. Both the theoretical and experimental results show that the acceleration amplitude increases as the freeplay gap increases. It is also seen that the peak location is almost independent of the freeplay gap values both for the theoretical and experimental results. The second peak amplitude is created by the wing structural nonlinearity and second gust angle excitation. For the store pitch response, there is a no second harmonic component. This means that the second harmonic component is dominated by only the wing bending mode. The quantitative agreement is reasonably good except near the resonant frequency, $\omega_g = 14$–$15\,\mathrm{Hz}$.

Figs. 20(a) and (b) show the typical measured time responses of the wing acceleration (a), the store pitch angle (b) for $U = 18.5\,\mathrm{m/s}$, $\omega_g = 11.9\,\mathrm{Hz}$ and the freeplay gap, $d = 0.5$. Note that for the store pitch response with freeplay gap as shown in Fig. 20(b), the present measured store pitch data only provide qualitative information. The store pitch response has a steady vibration around two equilibrium positions. The theoretical time histories corresponding to Figs. 20(a) and (b) are shown in Figs. 20(c) and (d). The FFT analysis corresponding to Figs. 20(a)–(d) is shown in Figs. 20(e) and (f). The dominant frequency response

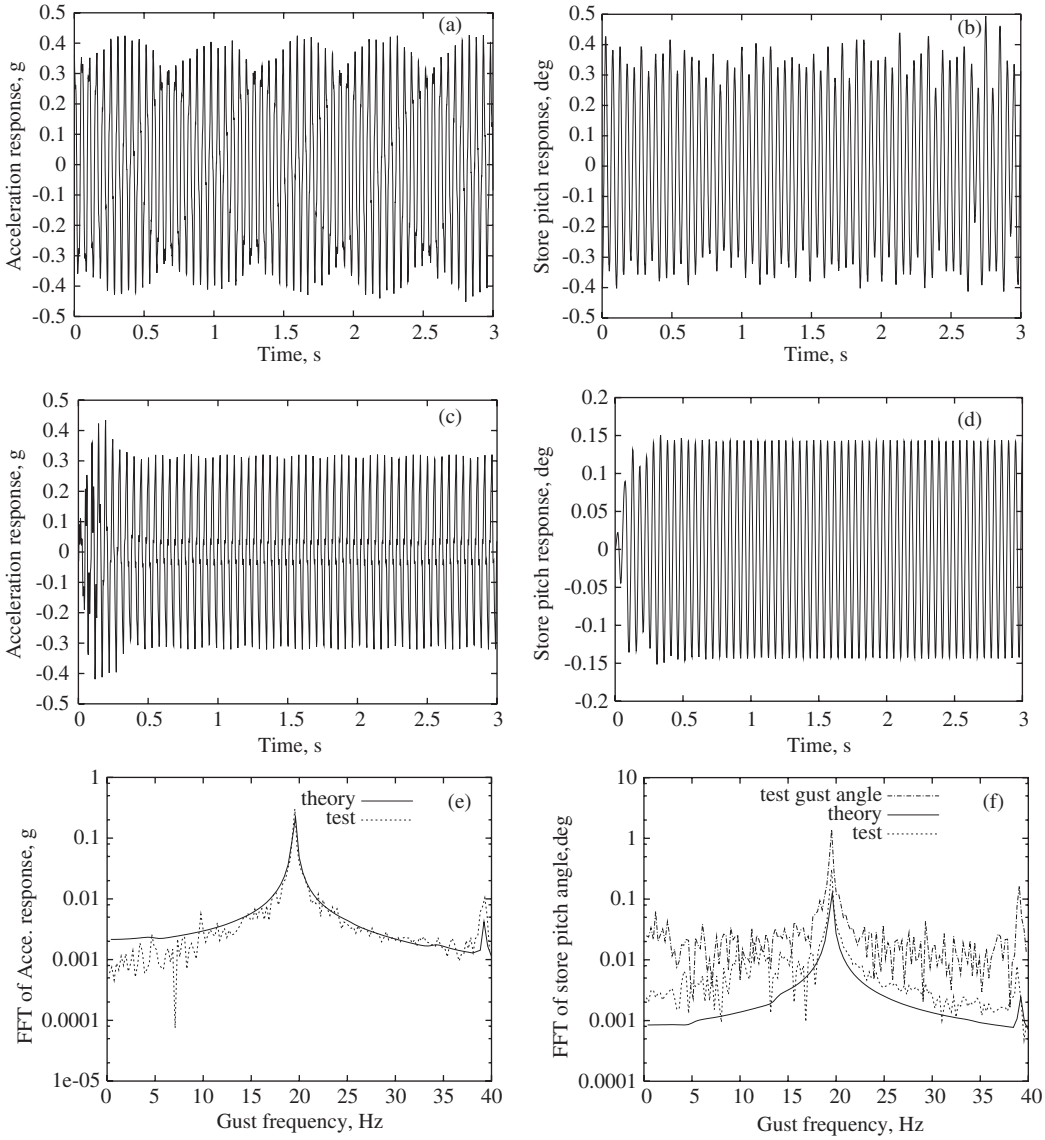

Fig. 17. Theoretical and experimental wing and store pitch responses for $U = 10\,\mathrm{m/s}$, $d = 0$ and $\omega_g = 19.5\,\mathrm{Hz}$: (a) measured wing response, (b) measured store pitch response, (c) theoretical wing response, (d) theoretical store response, (e) FFT of wing response; solid line, theory; dashed line, test; (f) FFT of store response; solid line, theory; dashed line, test; dashed point line, test gust angle.

component is located at the frequency, $\omega_g = 11.9\,\mathrm{Hz}$ and there are detectable $2\omega_g$ and $3\omega_g$ frequency components in addition to a dominant ω_g component. The $2\omega_g$ frequency component is excited by the second gust frequency component as well the structural nonlinearity of the wing, and the $3\omega_g$ frequency component is created by the structural nonlinearity of the wing. The theoretical $3\omega_g$ frequency component is stronger than the $2\omega_g$ frequency component. However, the experimental $3\omega_g$ frequency component is weaker than the $2\omega_g$ frequency component. This means the actual wing structure does not have so strong a structural nonlinearity as described by the von Karman plate theory.

For analysis of the wing dynamic response, a measured gust excitation time history for $U = 18.5\,\mathrm{m/s}$, $\omega_g = 11.9\,\mathrm{Hz}$ is shown in Fig. 18(b). The corresponding FFT analysis of this gust excitation is also plotted in Fig. 20(f). The dominant amplitude of the gust angle is $\alpha_{g1} = 1.24^\circ$ and the second gust amplitude is

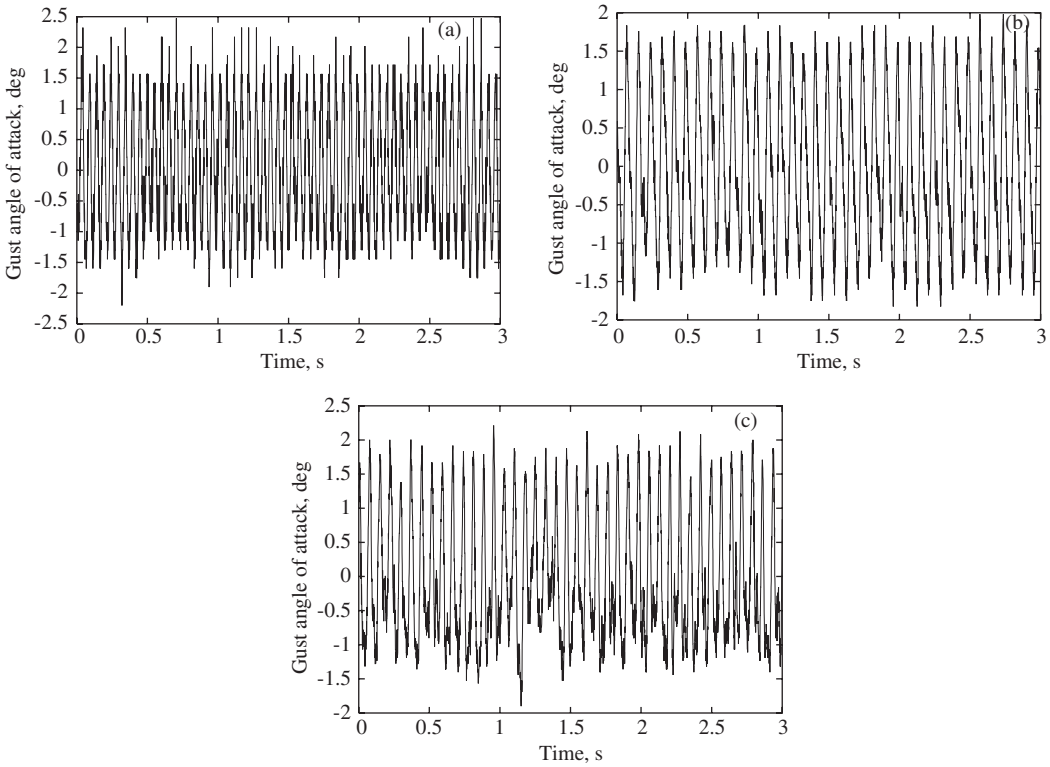

Fig. 18. Measured time histories of the gust angle of attack: (a) $U = 10\,\mathrm{m/s}$, $\omega_g = 19.5\,\mathrm{Hz}$, (b) $U = 18.5\,\mathrm{m/s}$, $\omega_g = 11.9\,\mathrm{Hz}$, (c) $U = 28\,\mathrm{m/s}$, $\omega_g = 13.6\,\mathrm{Hz}$.

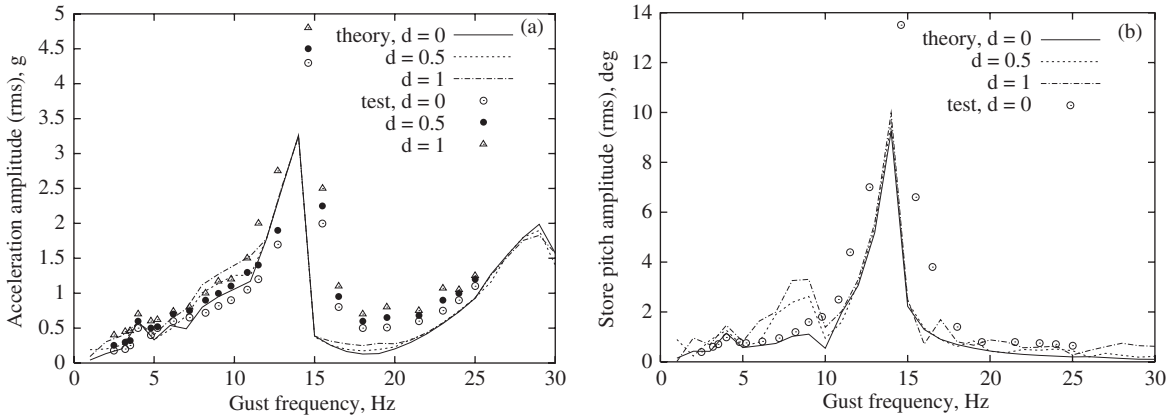

Fig. 19. Theoretical and experimental gust frequency response for $U = 18.5\,\mathrm{m/s}$, and the several freeplay gaps, $d = 0$, 0.5 and 1: (a) wing tip frequency response, (b) store pitch frequency response; ○, test, $d = 0$; ●, test, $d = 0.5$; △, test, $d = 1.0$; solid line, theory, $d = 0$; dashed line, theory, $d = 0.5$; dashed point line, theory, $d = 1.0$.

$\alpha_{g2} = 0.19^\circ$. There is noise in the gust excitation, thus it enlarges the difference between the theory and experiment.

When the freeplay gap and gust frequency increase from $d = 0.5$ to 1.0 and $\omega_g = 11.9$ to $\omega_g = 23\,\mathrm{Hz}$, the results are shown in Figs. 21(a)–(f). It is found that the theoretical and experimental wing acceleration

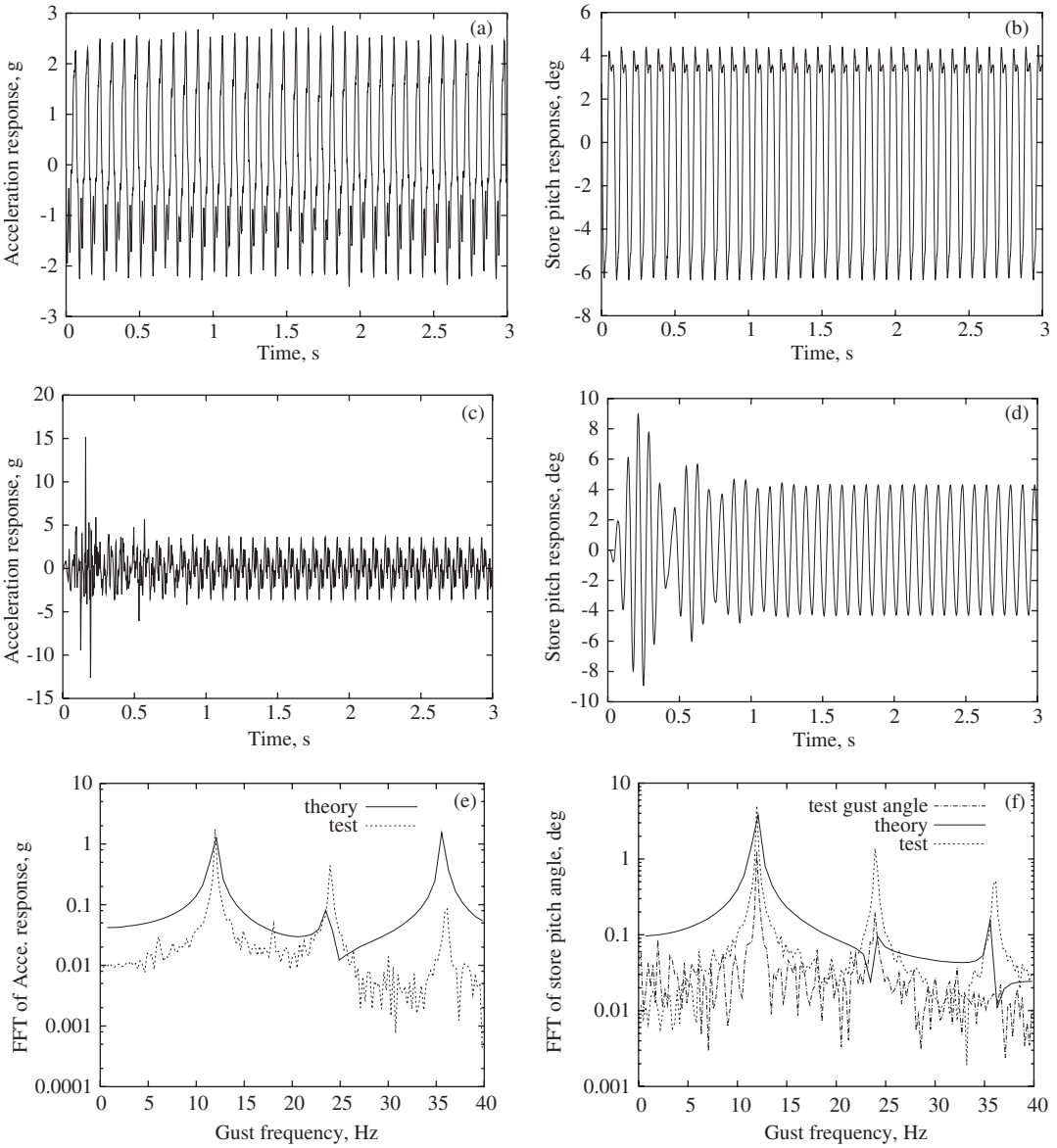

Fig. 20. Theoretical and experimental wing and store pitch responses for $U = 18.5\,\mathrm{m/s}$, $d = 0.5$ and $\omega_g = 11.9\,\mathrm{Hz}$: (a) measured wing response, (b) measured store pitch response, (c) theoretical wing response, (d) theoretical store response, (e) FFT of wing response; solid line, theory; dashed line, test; (f) FFT of store response; solid line, theory; dashed line, test; dashed point line, test gust angle.

responses are basically periodic with the dominant frequency component at 23 Hz as shown in Fig. 21(e), but both the theoretical and experimental store pitch responses are chaotic. There is a relatively broad frequency band width near the lower frequency components and the energy spectrum is not small as shown in Fig. 21(f).

Figs. 22(a) and (b) show the wing acceleration and the store pitch angle frequency responses for a flow velocity $U = 28\,\mathrm{m/s}$, that is larger than the linear flutter velocity. The symbols for the theoretical and experimental results are the same as before. For Fig. 22(a), there is a very obvious theoretical peak amplitude at the gust frequency, $\omega_g = 19\,\mathrm{Hz}$ for no freeplay gap ($d = 0$), $\omega_g = 18\,\mathrm{Hz}$ for the freeplay gaps, $d = 0.5$ and 1.0. These frequencies are the dominant resonant frequencies for the nonlinear system. The second wing peak amplitude is near $\omega_g = 36\,\mathrm{Hz}$, but does not appear in the store pitch response. The reason is the same as described in Fig. 19(b). The wing rms amplitude has a slight change when the freeplay gap increases from

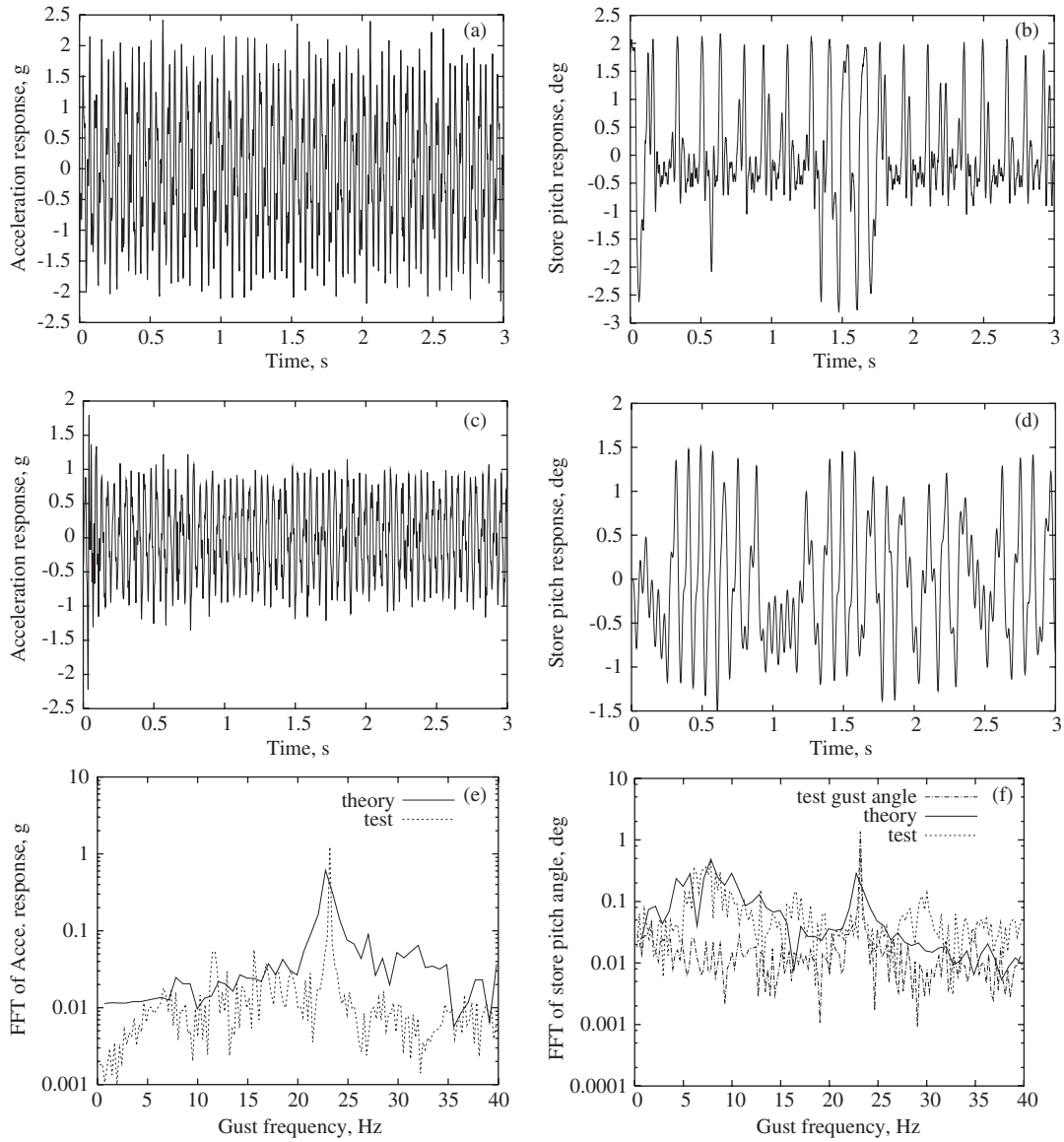

Fig. 21. Theoretical and experimental wing and store pitch responses for $U = 18.5\,\mathrm{m/s}$, $d = 1.0$ and $\omega_g = 23\,\mathrm{Hz}$: (a) measured wing response, (b) measured store pitch response, (c) theoretical wing response, (d) theoretical store response, (e) FFT of wing response; solid line, theory; dashed line, test; (f) FFT of store response; solid line, theory; dashed line, test; dashed point line, test gust angle.

$d = 0$ to 1 for both the theory and experiment. This because the store pitch angle response has a smaller change when the flow velocity is higher as shown in Fig. 22(b).

Large LCO are observed in the case of no gust excitation for $U = 28\,\mathrm{m/s}$. The rms amplitude at the wing mid-span of the trailing edge is 0.11 g for $d = 0$, 0.08 g for $d = 0.5$ and 0.07 g for $d = 1.0$ or the nondimensional wing displacement is 0.2, for $d = 0$, 0.1 for $d = 0.5$ and 0.08 for $d = 1.0$. To protect the experimental model from a very large dynamic response, only a few gust excitation frequencies are chosen. In general, the quantitative agreement between the theory and experiment is reasonably good.

When the gust frequency is higher, such as $\omega_g = 39\,\mathrm{Hz}$, the acceleration amplitude, 0.65 g, is larger than the LCO amplitude (0.11 g) for the no gust case, but the nondimensional wing displacement is about 0.07 which is smaller than the LCO amplitude (0.2). This phenomenon is observed in both the present theoretical and

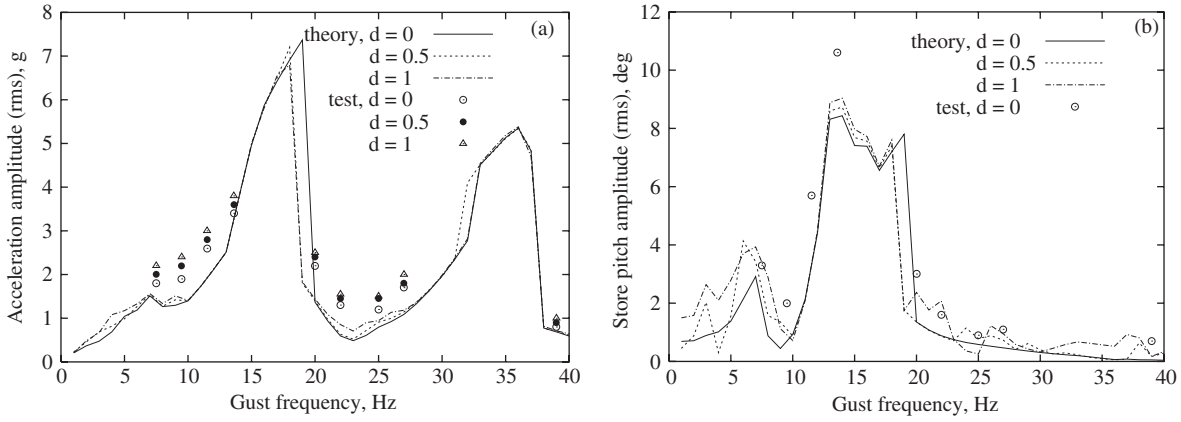

Fig. 22. Theoretical and experimental gust frequency response for $U = 28\,\mathrm{m/s}$, and the several freeplay gaps, $d = 0$, 0.5 and 1: (a) wing tip frequency response, (b) store pitch frequency response; ○, test, $d = 0$; ●, test, $d = 0.5$; △, test, $d = 1.0$; solid line, theory, $d = 0$; dashed line, theory, $d = 0.5$; dashed point line, theory, $d = 1.0$.

experimental data. When a gust angle of attack is smaller, this phenomenon is especially evident as shown in Fig. 4 for $\alpha_{g0} = 0.1^\circ$. It appears that a weak gust excitation with a high frequency can diminish the LCO amplitude.

Figs. 23(a) and (b) show the typical measured time responses of the wing acceleration (a), and the store pitch angle (b) for $U = 28\,\mathrm{m/s}$, $\omega_g = 13.6\,\mathrm{Hz}$ and the freeplay gap, $d = 1.0$. The store pitch response has a steady vibration around two equilibrium positions and the wing response is a periodic motion. The theoretical time responses corresponding to Figs. 23(a) and (b) are shown in Figs. 23(c) and (d). The FFT analysis corresponding to Figs. 23(a)–(d) is shown in Figs. 23(e) and (f). The measured gust angle of attack for $U = 28\,\mathrm{m/s}$, $\omega_g = 13.6\,\mathrm{Hz}$ is shown in Fig. 18(c) and the corresponding FFT analysis is also plotted in Fig. 23(f). The dominant amplitude of the gust angle is $\alpha_{g1} = 1.3^\circ$ and the second gust amplitude is $\alpha_{g2} = 0.21^\circ$.

As shown in Fig. 23(e), the dominant wing frequency response component is at the frequency $\omega = 13.6\,\mathrm{Hz}$ but the higher harmonic components are not small. The results are very similar to those for $u = 18.5\,\mathrm{m/s}$, but the responses are dominated by the periodic motion.

6. Concluding remarks

The nonlinear gust response of a delta wing with an external store model are studied using von Karman plate theory, a component modal analysis and a 3-D time domain vortex lattice aerodynamic model including a reduced order model aerodynamic technique. Results are computed for different freeplay gap values.

The theoretical results have been compared to experiment. The theoretical and experimental results show that the wing gust response is significantly dependent on the store pitch motion and the gust angle of attack. In general, the wing gust response amplitude increases as the freeplay gap or the gust angle increases and are almost independent of the store pitch initial conditions. It is interesting to note that when the flow velocity is beyond the linear flutter velocity, a smaller amplitude response is obtained for higher frequency gust excitation. Such behavior can only occur in a nonlinear dynamic system. In principle this effect can be used to alleviate the LCO response.

The quantitative correlations between the theory and experiment are reasonably good, but in the range of the dominant resonant frequency of this nonlinear system, i.e. at larger response amplitude, the correlations are not good. The theoretical model needs to be improved using a higher-order structural model as described in Ref. [24].

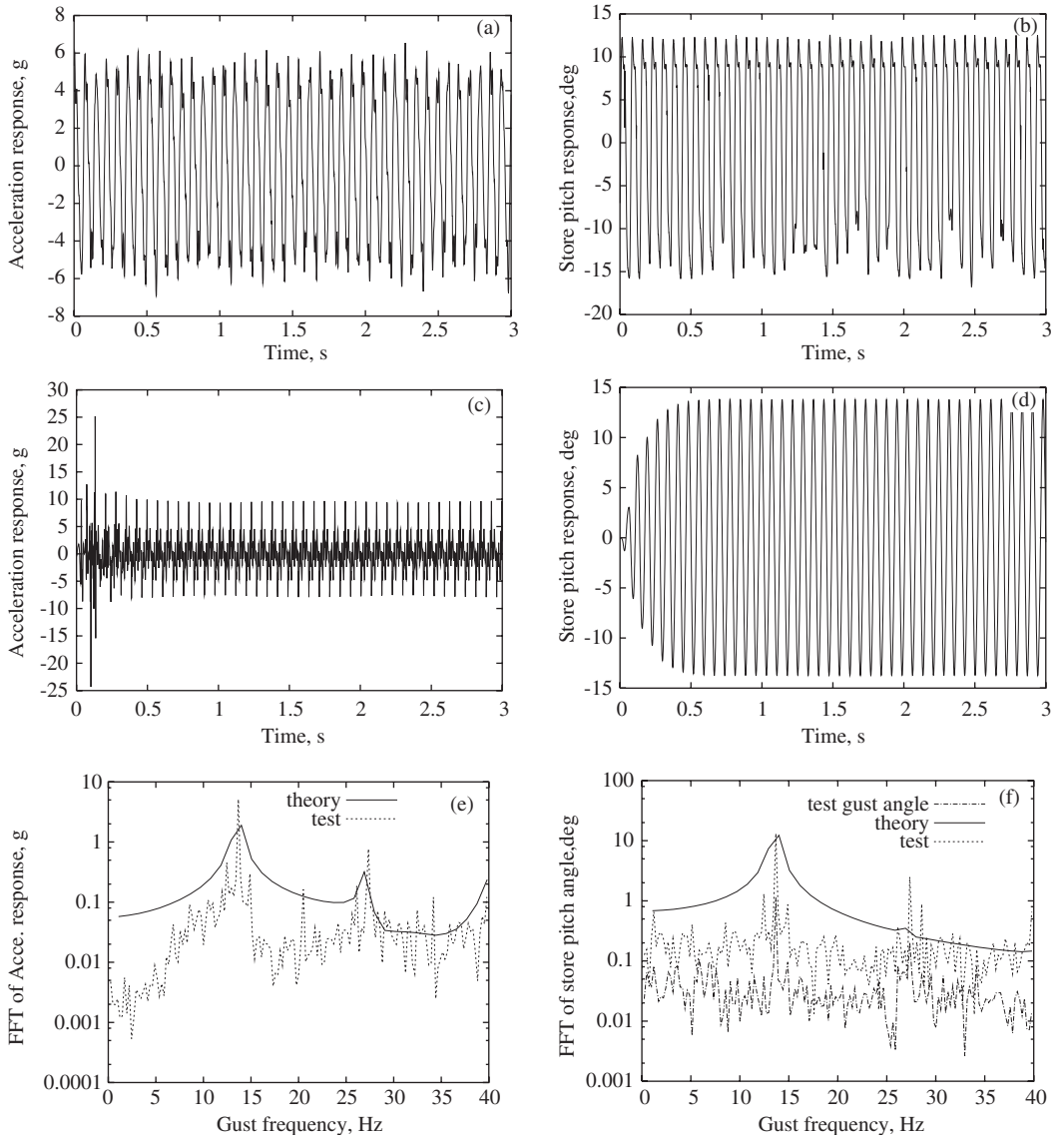

Fig. 23. Theoretical and experimental wing and store pitch responses for $U = 28\,\mathrm{m/s}$, $d = 1.0$ and $\omega_g = 13.6\,\mathrm{Hz}$: (a) measured wing response, (b) measured store pitch response, (c) theoretical wing response, (d) theoretical store response, (e) FFT of wing response; solid line, theory; dashed line, test; (f) FFT of store response; solid line, theory; dashed line, test; dashed point line, test gust angle.

Acknowlegments

This work was supported under AFOSR Grant, "Dynamic and Control of Nonlinear Fluid-Structure Interaction" under the direction of Drs Dean Mook and Tom Kim. We would like to thank graduate student Sid Rupani for his participation in the data acquisition phase of the wind tunnel test.

References

[1] E.H. Dowell, J. Edwards, T. Strganac, Nonlinear aeroelasticity, *Journal of Aircraft* 40 (5) (2003) 857–874.
[2] J.G. Jones, Statistical discrete gust theory for aircraft loads, Royal Aircraft Establishment, TR 73167, November 1973.

[3] B. Perry III, A.S. Pototzky, J.A. Woods, NASA investigation of a claimed "Overlap" between two gust response analysis methods, *Journal of Aircraft* 27 (7) (1990) 606–611.
[4] C.L. Pettit, R.V. Grandhi, Optimization of a wing structure for gust response and aileron effectiveness, *Journal of Aircraft* 40 (6) (2003) 1185–1191.
[5] X. Luo, R.V. Grandhi, ASTROS for reliability-based multidisciplinary structural analysis and optimization, *Computers and Structures* 62 (4) (1997) 737–745.
[6] M. Karpel, Design for active flutter suppression and gust alleviation using state-space aeroelastic modeling, *Journal of Aircraft* 19 (3) (1982) 221–227.
[7] D.M. Tang, P.G.A. Cizmas, E.H. Dowell, Experiments and analysis for a gust generator in a wind tunnel, *Journal of Aircraft* 33 (1) (1996) 139–148.
[8] D.M. Tang, D. Kholodar, E.H. Dowell, Nonlinear aeroelastic response of a airfoil section with control surface freeplay to gust loads, *AIAA Journal* 38 (9) (2000) 1543–1557.
[9] D.M. Tang, H.P. Gavin, E.H. Dowell, Study of airfoil gust response alleviation using an electro-magnetic dry friction damper—part 1: theory, *Journal of Sound and Vibration* 269 (2004) 853–874.
[10] D.M. Tang, H.P. Gavin, E.H. Dowell, Study of airfoil gust response alleviation using an electro-magnetic dry friction damper—part 2: experiment, *Journal of Sound and Vibration* 269 (2004) 875–897.
[11] D.M. Tang, E.H. Dowell, Experimental and theoretical study of gust response for a high-aspect ratio wing, *AIAA Journal* 40 (3) (2002) 419–429.
[12] D.M. Tang, E.H. Dowell, Nonlinear response of a non-rotating rotor blade to a periodic gust, *Journal of Fluids and Structures* 10 (1996) 721–742.
[13] D.M. Tang, E.H. Dowell, Response of a non-rotating rotor blade to lateral turbulence in sinusoidal pulsating flow—part 1: theory, *Journal of Aircraft* 32 (1) (1995) 145–153.
[14] D.M. Tang, E.H. Dowell, Response of a non-rotating rotor blade to lateral turbulence in sinusoidal pulsating flow—part 2: experiment, *Journal of Aircraft* 32 (1) (1995) 154–160.
[15] D.M. Tang, J.K. Henry, E.H. Dowell, Nonlinear aeroelastic response of delta wing to periodic gust, *Journal of Aircraft* 37 (1) (2000) 155–164.
[16] D.M. Tang, J.K. Henry, E.H. Dowell, Effects of steady angle of attack on nonlinear gust response of a delta wing model, *Journal of Fluids and Structures* 16 (8) (2002) 1093–1110.
[17] D.M. Tang, P. Attar, E.H. Dowell, Flutter/LCO analysis and experiment for a wing–store model—part I: with von Karman plate theory, *AIAA Journal*, 2006, to appear.
[18] D.M. Tang, E.H. Dowell, Flutter and limit cycle oscillations for of a wing–store model with freeplay, *Journal of Aircraft*, 2006, to appear.
[19] B.H. Tongue, E.H. Dowell, Component modal analysis of nonlinear, nonconservative system, *ASME Journal of Applied Mechanics* 50 (1983) 204–209.
[20] ANSYS User Manual, Release 5.5.1, Swanson Analysis Systems, Inc., 1998.
[21] K.C. Hall, Eigenanalysis of unsteady flows about airfoils, cascades, and wings, *AIAA Journal* 32 (12) (1994) 2426–2432.
[22] R.L. Bisplinghoff, H. Ashley, R.L. Halfman, *Aeroelasticity*, Addison-Wesley, Reading, MA, 1955.
[23] E.H. Dowell, K.C. Hall, Modeling of fluid–structure interaction, *Annual Reviews of Fluid Mechanics* 33 (2001) 445–490 (Invited Chapter).
[24] P. Attar, E.H. Dowell, D.M. Tang, Modeling the LCO of a delta wing with an external store using a high fidelity structural model, *Presented at the 2005 AIAA SDM Conference*, Austin, TX, April 2005.